Upper ocean temperature characteristics in the subantarctic Southeast Pacific based on biomarker reconstructions

Julia R. Hagemann[1], Lester Lembke-Jene[1], Frank Lamy[1], Maria-Elena Vorrath[2], Jérôme Kaiser[3], Juliane Müller[1], Helge W. Arz[3], Jens Hefter[1], Andrea Jaeschke[4], Nicoletta Ruggieri[1], Ralf Tiedemann[1]

[1]Alfred Wegener Institute, Helmholtz Centre for Polar and Marine Research, 27570 Bremerhaven, Germany
[2]Institute for Geology, University Hamburg, 20146 Hamburg, Germany
[3]Leibniz-Institute for Baltic Sea Research Warnemünde, 18119 Rostock, Germany
[4]Institute of Geology and Mineralogy, University of Cologne, 50923 Cologne, Germany
^

Correspondence to: Julia. R. Hagemann (Julia.Hagemann@awi.de) and Lester Lembke-Jene (Lester.Lembke-Jene@awi.de)

Abstract. Alkenones and isoprenoid Glycerol Dialkyl Glycerol Tetraether lipids (isoGDGT) as remnants of living organisms are widely used biomarkers for determining past oceans' water temperatures. The organisms these proxy carriers stem from, are influenced by a number of environmental parameters, such as water depth, nutrient availability, light conditions or seasonality, which all may significantly bias the calibration to ambient water temperatures. Reliable temperature determinations remain thus challenging, especially in higher latitudes and for under-sampled regions. We analyzed 33 sediment surface samples from the Southern Chilean continental margin and the Drake Passage for alkenones and isoGDGTs and compared the results with gridded instrumental reference data from the World Ocean Atlas 2005 (WOA05), as well as previously published data from an extended study area covering the Central and Western South Pacific towards the New Zealand continental margin. We show that for alkenone-derived Sea Surface Temperatures (SST), the widely-used global core-top calibration of Müller et al. (1998) yields the smallest deviation of the WOA05-based SSTs. The calibration of Sikes et al. (1997) instead, adapted to higher latitudes and supposed to show summer SSTs, overestimates modern WOA05-based SSTs. Our alkenone SSTs show a slight seasonal shift of ~1° C at the Southern Chilean Margin and up to ~2° C in the Drake Passage towards austral summer SSTs. Samples in the Central South Pacific on the other hand reflect an annual mean signal. We show that for isoGDGT-based temperatures the subsurface calibration of Kim et al. (2012a) best reflects temperatures from the WOA05 in areas north of the Subantarctic Front (SAF). Temperatures south of the SAF in contrast are significantly overestimated by up to 14° C, irrespective of the applied calibration. In addition, we used the GDGT [2]/[3]-ratios, which gives an indication of the production depth of the isoGDGTs and/or potentially influences from land. Our samples reflect a subsurface (0 to 200 m water depth) rather than a surface (0 – 50 m water depth) signal in the entire study area and show a correlation with the monthly dust distribution in the South Pacific, indicating terrigenous influences. The overestimation of isoGDGTs surface and subsurface temperatures south of the SAF highlights the need for a re-assessment of existing calibrations in the polar Southern Ocean. Therefore, we suggest a modified Southern Ocean TEX^{L}_{86} – based calibration for

surface and subsurface temperatures, which shows a lower temperature sensitivity and yields principally lower absolute temperatures, which align more closely with WOA05-derived values and also OH-isoGDGT-derived temperatures.

1 Introduction

Alkenones (e.g., Brassell et al., 1986; Herbert, 2001, 2014) and isoGDGTs (isoprenoid Glycerol Dialkyl Glycerol Tetraether; Schouten et al., 2002; Schouten et al., 2013a) are widely used for determining oceans' past water temperatures. These biomarkers are present in all oceans and occur from the tropics to high latitudes (e.g., Herbert et al., 2010; Sikes et al., 1997; Müller et al., 1998; Conte et al., 2006). Alkenone-derived sea surface temperatures (SSTs) are based on lipid remains of photoautotrophic Coccolithophorids (e.g., Baumann et al., 2005; Brassell et al., 1986). The ratio of di- and tri-unsaturated alkenones, expressed as the Unsaturation Ketone index $U^{K'}_{37}$ (**Table A1**) is reflecting SSTs (Prahl and Wakeham, 1987). Calculation of SSTs is based on calibration equations developed over the past ~40 years (**Table A1**). Most of these empirically-derived equations are relatively similar, and based on comparison of either culture experiments (Prahl et al., 1988; Prahl and Wakeham, 1987) or surface sediment samples from tropical to subpolar regions with corresponding instrumental data (Müller et al., 1998). Other calibrations (e.g., Sikes et al., 1997) were developed specifically for (sub)polar regions and are adapted for a seasonal bias toward summer SSTs. Henceforth, we use the terms Müller98 for the calibration by Müller et al. (1998) and Sikes97 for the calibration by Sikes et al. (1997; **Table A1**).

The accuracy of alkenone-based calibrations can be influenced by other environmental factors besides temperature, such as light levels, changes in growth rate or nutrient availability, but none of these factors seems to have an appreciable effect on the $U^{K'}_{37}$ index (e.g., Caniupán et al., 2014; Epstein et al., 2001; Herbert, 2001; Müller et al., 1998; Popp et al., 1998). In contrast, preferential degradation of the alkenone $C_{37:3}$ in sediment under aerobic conditions may bias the $U^{K'}_{37}$ signal towards warmer SSTs (Prahl et al., 2010). Seasonality often plays a significant role at high latitudes (e.g., Max et al., 2020; Prahl et al., 2010), due to primary production being more pronounced in the thermal summer season and annual temperature differences that increases with increasing latitude. In our study region, samples from the Central South Pacific most likely represent either summer temperatures (with the Sikes97 calibration) or an annual mean (Müller98 calibration; Jaeschke et al., 2017). Prahl et al. (2010), using samples from the Chilean continental slope, found a slight seasonal summer bias south of ~50° S. In contrast, studies from the North Pacific show a seasonal signal towards late summer to autumn SSTs that differ from the annual mean by up to 6° C (e.g., Max et al., 2020; Prahl et al., 2010).

IsoGDGTs are lipid remains of *Thaumarchaeota* (formerly called Crearchaeota Group I; Brochier-Armanet et al., 2008) that include a certain number of moieties, which increases with growth temperature (Schouten et al., 2002). The lipids GDGT-0; GDGT-1; GDGT-2; GDGT-3 contain zero to three cyclopentane moieties in their molecule structure, whereas Crenarchaeol and its isomer Cren' feature four cyclopentane and one hexane moieties. These ring structures regulate membrane fluidity of *Thaumarchaeota* and change as an adaption to their ambient temperature (Chong, 2010; Gabriel and Chong, 2000; Schouten et al., 2002). Determination of isoGDGT-derived water temperatures is based on the Tetraether index (TEX_{86}; Schouten et al.,

Deleted: Table A1
Formatted: Font: Bold
Formatted: Font: Bold
Deleted: Table A1
Formatted: Font: Bold
Formatted: Font: Bold
Deleted: The number of moieties

2002), or their modifications TEX^{H}_{86} and TEX^{L}_{86} (**Table A1**), which have been determined for water temperatures >15° C and <15° C, respectively (Kim et al., 2010). While TEX^{H}_{86} is a logarithmic function of the original index, TEX^{L}_{86} omits the GDGT-3 from the denominator and removes the isomer Cren' from the equation, due to a weaker correlation to water temperatures in cold regions (Kim et al., 2010). In addition to cyclopentane moieties, three OH-isoGDGTs may also contribute to ambient temperature adaption (OH-isoGDGT-0, OH-isoGDGT-1, and OH-isoGDGT-2). These OH-isoGDGTs occur globally, but in higher amounts in the polar regions, as further adaption of the *Thaumarchaeota* to the cold environment (Fietz et al., 2013; Huguet et al., 2013; Liu et al., 2020). OH-isoGDGTs are frequently so important in polar regions or during glacial phases that it has been recommended to include them in temperature calibrations (Fietz et al., 2020; Fietz et al., 2016). In contrast to photo-autotrophic coccolithophores, *Thaumarchaeota* occur throughout the water column (Karner et al., 2001), which complicates the attribution of the reconstructed temperature signal to specific water depths. In general, it is assumed that *Thaumarchaeota* predominantly reflect either a subsurface, i.e., seasonal mixed-layer temperature (Tsub; 0 – 200 m water depth), or an SST signal (**Table A1**), because the grazing and repacking of isoGDGTs into fecal pellets occurs most effectively within the photic zone (Wuchter et al., 2005). The GDGT [2]/[3]-ratio can be used to roughly determine the habitat depth of the *Thaumarchaeota*, since it increases with increasing water depth (Dong et al., 2019; Hernández-Sánchez et al., 2014; Kim et al., 2015; Kim et al., 2016; Schouten et al., 2012; Taylor et al., 2013). For the subpolar and polar Southern Ocean, in particular the extensive SE Pacific sector, only little information exists to date about the applicability of these different temperature proxies and their respective calibrations. In addition, systematic comparisons between alkenone and isoGDGT-based temperature reconstructions using surface sediments have thus far been limited (e.g., Jaeschke et al., 2017; Kaiser et al., 2015). We use the terms SST^{H}Kim and SST^{L}Kim for the two global surface calibrations by Kim et al. (2010), $Tsub^{H}$Kim and $Tsub^{L}$Kim for the two global subsurface calibrations by Kim et al. (2012a, 2012b) and SST^{H}Kaiser and $Tsub^{H}$Kaiser for the local surface and subsurface calibration by Kaiser et al. (2015; **Table A1**).

In this study, we present a new set of 33 sediment surface samples located along the Southern Chilean Margin (SCM) and the Drake Passage (DP; ~52 – 62° S) to determine upper ocean water temperatures based on alkenones ($U^{K'}_{37}$) and isoGDGTs (TEX^{H}_{86} and TEX^{L}_{86}). We compare our regional results with previously published data from an extended, temperate to subpolar South Pacific study area (**Figure 1**).

We assess the applicability of the Müller98 and Sikes97 calibrations with World Ocean Atlas (WOA05)-based temperatures and investigate the influence of seasonality on alkenone-based temperature reconstructions. Furthermore, we compare the isoGDGT-based indices TEX^{H}_{86} and TEX^{L}_{86} and their most common calibrations for SST and Tsub (**Table A1**) with WOA05-based temperatures. Lastly, we check the potential influence of habitat depth on signal incorporation on the basis of the GDGT [2]/[3]-ratio and propose a new calibration specifically for the polar Pacific sector of the Southern Ocean (SO) south of the Subantarctic Front.

Deleted: Table A1
Formatted: Font: Bold
Formatted: Font: Bold
Deleted: Table A1
Formatted: Font: Bold
Formatted: Font: Bold
Deleted: based on
Deleted: Table A1
Formatted: Font: Bold
Formatted: Font: Bold

2 Study Area

Our study area comprises the subpolar and polar SE Pacific sector of the SO, including the Drake Passage (**Figure 1**). One important characteristic of the SO is the eastward-flowing Antarctic Circumpolar Current (ACC), which is largely driven by Southern Westerly Winds (SWW) and buoyancy forcing (Rintoul, 2018; Watson et al., 2015). The ACC flows unimpeded around Antarctica, and is only slowed down by the South American continent (Orsi et al., 1995), where the northern branch of the ACC bifurcates at ~40 – 45° S into the northward-flowing Peru-Chile Current (PCC) and the southward-flowing Cape Horn Current (CHC; Strub et al., 1998). CHC and ACC jointly transport ca. 130 – 150 Sv of water (e.g., Koenig et al., 2014) through the ~800 km wide Drake Passage into the Atlantic Ocean (**Figure 1**).

Several fronts within the ACC characterize the convergence of water masses that differ in temperature, salinity and nutrient content (Orsi et al., 1995). The northern boundary of the ACC is defined by the Subtropical Front (STF; Orsi et al., 1995), followed from north to south by the Subantarctic Front (SAF), the Polar Front (PF) and the Southern ACC Front (SACCF). Apart from the STF, which is interrupted by the South American continent, all three fronts (SAF, PF and SACCF) pass through the Drake Passage (Orsi et al., 1995; **Figure 1**). The zones between the fronts are defined as areas with differing temperature and salinity characteristics, both decreasing with increasing latitude. The SAF marks the beginning of the Antarctic Intermediate Water's (AAIW) northward descent to a depth of ~500 m. AAIW itself is associated with a salinity minimum of <34 PSU. The PF, on the other hand, marks the northern temperature limit of the cold Antarctic surface water. The SACCF instead has no distinct separating features in the surface water. The boundary is here defined along the mesopelagic temperature maximum of the upwelled Upper Circumpolar Deep Water (UCDW; Orsi et al., 1995 and references therein).

3 Material and Methods

A total amount of 33 Multi-Corer (MUC) samples (**Table A2**) along the Southern Chilean Margin and the Drake Passage were analyzed for alkenones and isoGDGTs. The samples were collected during R/V Polarstern expedition PS97 in February-April 2016 (Lamy, 2016) along a latitudinal transect on the Southern Chilean Margin and through the Southern Ocean frontal system.

The MUC samples were stored deep-frozen immediately after sampling onboard and freeze-dried afterwards in the laboratory. Extraction of the biomarkers was carried out with two different approaches. Between 3 and 5 g of ground surface sediment (0 – 1 cm) from each site was extracted either by an accelerated Solvent Extraction (DIONEX ASE 350; Thermo Scientific) with DCM:MeOH (9:1, v:v) for the samples of the Chilean margin (including three samples from the Drake Passage) or in an ultrasonic bath with DCM:MeOH (2:1, v:v) for the samples of the Drake Passage. As internal standard, 100 µl each of the *n*-alkane C_{36} or 2-nonadecanone standard and C_{46} were added before extraction. The two data sets were initially used to address differing research objectives. The samples from the Chilean margin (including three DP samples) were primarily used for extracting alkenones for SST. Previous works on the DP samples, on the other hand, focused on highly branched isoprenoids (HBIs), sterols and isoGDGTs (Lamping et al., 2021; Vorrath et al., 2020), and were extracted using sonication as a lower recovery of higher unsaturated HBIs is known when using the ASE method (Belt et al., 2014). In contrast, the TEX_{86}

Deleted: Table A2

Formatted: Font: Bold

Formatted: Font: Bold

index does not appear to be substantially affected by extraction techniques (Schouten et al., 2013b). The good agreement between the three ASE extraction DP samples and the ultrasonic bath samples (**Figure 7D – F**) suggests that the two data sets are comparable.

The bulk of the solvent was removed by rotary evaporation, under a nitrogen gas stream or in a Rocket Evaporator (Genevac – SP Scientific). The different fractions were chromatographically separated using small glass columns filled with 5 cm of activated silicagel. After adding the sample, the column was rinsed with 5 ml *n*-hexane, 5 ml or 8 ml *n*-hexane:DCM (1:1, v:v), 5 ml DCM and 4 ml DCM:MeOH (1:1, v:v) to yield *n*-alkanes, alkenones and isoGDGTs, respectively. The samples were dried again and transferred into 2 ml vials. For the measurement, the alkenone fractions were diluted with 200 – 20 µl *n*-hexane, the GDGT fraction was filtered first, and then diluted with 50 – 120 µl *n*-hexane:isopropanol (99:1, v:v).

Alkenones were injected with 1 µl solvent and Helium as carrier gas into an Agilent HP6890 Gas Chromatograph equipped with a 60 m DB-1 MS column and a flame ionization detector. The oven temperature was increased from initially 60° C to 150° C with 20° C min^{-1} and thereafter with 6° C min^{-1} until 320° C were reached.

For the GDGT measurements of most DP samples, we refer to the original studies by Lamping et al. (2021) and Vorrath et al. (2020). The other part of the GDGT samples were analyzed on an Agilent 1260 Infinity II ultrahigh-performance liquid chromatography-mass spectrometry (UHPLC-MS) system and a G6125C single quadrupole mass spectrometer. The chromatographic separation was achieved by coupling two UPLC silica columns (Waters Acquity BEH HILIC, 2.1 × 150 mm, 1.7 µm) and a 2.1 × 5 mm pre-column as in Hopmans et al. (2016), but with the following chromatographic modifications: Mobile phases A and B consisted of *n*-hexane: chloroform (99:1, v/v) and *n*-hexane: 2-propanol: chloroform (89:10:1, v/v/v), respectively. The flow rate was set to 0.4 ml/min and the columns heated to 50° C, resulting in a maximum backpressure of 425 bar. Sample aliquots of 20 µl were injected with isocratic elution for 20 minutes using 86% A and 14% B, followed by a gradient to 30% A and 70% B within the next 20 min. After this, the mobile phase was set to 100% B and the column rinsed for 13 min, followed by 7 min re-equilibration time with 86% A and 14% B before the next sample analysis. The total run time was 60 min.

IsoGDGTs were detected using positive ion APCI-MS and selective ion monitoring (SIM) of $(M + H)^+$ ions (Schouten et al., 2007) with the following settings: nebulizer pressure 50 psi, vaporizer and drying gas temperature 350° C, drying gas flow 5 L/min. The capillary voltage was 4 kV and the corona current +5 µA. The detector was set for the following SIM ions: *m/z* 744 (C_{46} standard), *m/z* 1302.3 (GDGT-0), *m/z* 1300.3 (GDGT-1), *m/z* 1298.3 (GDGT-2), *m/z* 1296.3 (GDGT-3), *m/z* 1292.3 (Crenarchaeol and Cren' isomer). The resulting scan/dwell time was 66 ms.

4 Results and Discussion

Our samples are located on a meridional transect along the Chilean margin extending into the DP, with changing environmental conditions, in particular for SSTs, nutrients supply, salinity and current regimes. The $U^{K'}_{37}$ values range from 0.07 (PS97/079) to 0.38 (PS97/132), with minimum values in the southernmost region and increasing values to the north. All indices from alkenones and isoGDGTs are listed in **Table A2**. In **Chapter 4.1** and **4.2**, we compare the two most widely used calibrations for alkenones in this region: the subpolar and polar SO Sikes97 calibration, as well as the Müller98 calibration hereafter.

Deleted: Table A2
Formatted: Font: Bold, English (US)

4.1 Alkenone-based Sea Surface Temperatures

Alkenone-based SSTs calculated with Müller98 range from ~10° C in the northernmost locations of our study area to ~1° C in the southern part of the Drake Passage, south of the PF (**Figure 2A, B**). SST estimates based on Sikes97 instead range from ~12.5° C in the northernmost locations to ~4° C in the Drake Passage (**Figure 2C, D**). Most values fit closely to the Müller98 calibration line of both, annual mean and summer SSTs, but show an offset to the Sikes97 calibration line (**Figure 3**). Although Sikes97 was specifically adapted to the subpolar and polar SO, it generally overestimates modern SSTs in this study area, both for annual mean and summer (**Figure 2** and **Figure 3**). Our samples for the SE Pacific fit well to Müller98, but not to Sikes97 (**Figure 2** and **Figure 3**). Because of the latter's overestimation of modern temperatures, we hereafter chose to solely use the Müller98 calibration.

4.2 Influence of seasonality on alkenone temperature reconstruction

4.2.1 Seasonal signal along the Chilean Margin

Our alkenone-based SSTs fits WOA05-derived annual mean and summer temperatures and show only a small seasonal effect towards warmer SSTs. This observation is also in line with previous data from the Northern – Central Chilean Margin, which yields a slight seasonal effect south of 50° S (Prahl et al., 2006; Prahl et al., 2010). Also, a previous study from the Chilean fjord region confirms SST signals being only slightly shifted towards summer in the southern Chilean fjord region (**Figure 4**; Caniupán et al., 2014). Along the Chilean continental margin, this seasonal summer effect even further decreases southward to only ~1° C (i.e., summer SSTs vs. annual mean) between 50 – 57° S, based on WOA05-derived SSTs (**Figure 4**; blue and yellow cross). This deviation of 1° C, at least north of the SAF, is within the generally accepted error range for alkenone-derived paleo-SSTs of ±1.5° C (Müller et al., 1998), so that seasonality here appears to be negligible. Only further south in the Drake Passage, deviations of our reconstructed summer temperatures from the annual mean increase to about 2° C, which are likewise reflected in WOA05-based SSTs (**Figure 4**). Model results show a similar trend, with a small deviation from the annual mean of up to 2.5° C at higher latitudes as well (Conte et al., 2006). Such an increasing poleward seasonality is not unusual due to a temporal shift of the alkenone production towards summer (e.g., Volkman, 2000). Another effect that could be involved in the increased seasonality is the reduction in the diversity and quantity of coccolithophores through the frontal system of the ACC (e.g., Saavedra-Pellitero et al., 2014; Vollmar et al., 2022; Saavedra-Pellitero et al., 2019). The coccolithophore assemblages between the PF and the SAF show a significantly reduced diversity compared to north of the SAF. South of the PF, coccolithophorids occur only sporadically and show a reduced diversity (Saavedra-Pellitero et al., 2014). In this region, we are nearing the lower temperature end and thus ecological boundary conditions for coccolithophores. So,

Deleted: world ocean atlas
Deleted: , showing

alkenone production could be biased towards warmer years within the inevitably large time period of several hundreds of years that is comprised in the uppermost centimeter of surface sediment.

Not all data can be described by the poleward increase in the seasonal influence, since at two locations along the Chilean margin an annual mean temperature is reflected instead (**Figure 4**; red circles). The first region is located between ~54 – 58° S near the Strait of Magellan, where Atlantic waters mix with Pacific waters. The second region encompasses samples in the DP located close to the PF. The PF marks the temperature boundary of the cold Antarctic surface water, which is subducted at the PF and transported northwards (Orsi et al., 1995 - and references therein). This vertical water mass structure likely suppresses potential seasonal effects by providing homogenous temperatures throughout the annual cycle, due to a reduce opportunity to build up a warm summer surface layer.

Deleted: In addition, not all data uniformly show a seasonal trend. The poleward increasing seasonal trend is discontinued by two regions that reflect an annual mean instead

This weakly expressed seasonality in our results, which remains mostly within the error range of Müller98, is in stark contrast to results from other regions, notably the subarctic North Pacific. There, several studies showed a more consistent seasonal shift towards summer and autumn SSTs of 4 – 6° C north of the subarctic front, while locations south of the subarctic front reflect an annual mean (Max et al., 2020; Méheust et al., 2013; Prahl et al., 2010). The subarctic front in the North Pacific acts as a natural boundary, creating a highly stratified subarctic surface ocean with a permanent halocline and to pronounced seasonal summer warming within strongly stratified surface waters. In contrast, the transition in the South Pacific from subtropical to polar regions is characterized by a lower salinity gradient and stratification, leading to a less pronounced SAF. The year-round deep mixing within the ACC prevents the formation of a prominent warm water layer during the summer. Thus, subantarctic SSTs would be expected to show less seasonal influence on their SST signal.

Deleted: .

Deleted: In the South Pacific instead, t

Deleted: . As a result, the former likely leads to pronounced seasonal summer warming within strongly stratified surface waters, whereas the latter less stratified upper ocean would yield less pronounced warming during austral summer months

4.2.2 Regional synthesis of seasonality patterns across the South Pacific

We compared the samples from our relatively small study region with published data from the South Pacific Gyre, the Central South Pacific, the New Zealand Margin (Jaeschke et al., 2017) and the Northern – Central Chilean Margin (Prahl et al., 2006; Prahl et al., 2010) based on the Müller98 and Sikes97 calibrations (**Figure 5**). We also calculated the residual temperatures by subtracting the modern WOA05 temperatures at 10 m water depth from our calculated temperatures, shown in combination with $U^{K'}_{37}$ against SSTs (**Figure 5**). The Central South Pacific and New Zealand Margin samples of Jaeschke et al. (2017) spread over a wide area with different conditions. Taking into account a seasonal effect towards summer SSTs, only few samples of this extended data set match with the Sikes97 calibration (**Figure 5A, B**; Jaeschke et al., 2017). This is partly in contrast to Jaeschke et al. (2017) who concluded that alkenone-derived SSTs in general best reflect the austral summer months when using Sikes97 calibration. The Müller98 calibration is applicable in the entire extended study area when compared with both, annual mean and summer SSTs, reaffirming our decision to use Müller98 for further analyses.

The SCM and the Drake Passage samples are generally warmer by ~1.5° C than the samples from the Central South Pacific region (**Figure 6**). The Central South Pacific samples represent a best fit to annual mean, in contrast to the SCM and DP samples, which have a slight, but mostly negligible, seasonal shift toward summer SSTs (**Figure 6**). The most likely reason for this bias to summer SSTs in the SE-Pacific could be a higher nutrient availability during the summer months due to the close proximity of the SE Pacific samples to South America. High nutrient availability could lead to a potentially changing competition between different primary producers, e.g., high silica input favors a diatom bloom, which changes when silica is depleted (e.g., Durak et al., 2016; Smith et al., 2017; Tyrrell and Merico, 2004). In this region, nutrient input is expected to be highest during austral summer months, when the high precipitation rates of 3,000 – 10,000 mm/yr in South Patagonia reach their maximum (e.g., Garreaud et al., 2013; Lamy et al., 2010; Schneider et al., 2003). The increased precipitation during summer months results in an increased freshwater runoff (e.g., Dávila et al., 2002), accompanied by increased supply of continent-derived nutrients to hemipelagic and DP waters and a more stable seasonal thermocline (Toyos et al., 2022), which would both favor a seasonal coccolithophore bloom.

The area off New Zealand correlates well with samples off the Northern – Central Chilean Margin north of ~45° S and corresponds to the annual mean (**Figure 6**). In contrast, the South Pacific Gyre samples reflect a summer to autumn signal (**Figure 6**; Jaeschke et al., 2017). The South Pacific Gyre is characterized by extremely low nutrient content and accordingly low primary production (D'hondt et al., 2009). Reasons for the low nutrient content here are the distance from potential continental inputs, and a relatively deep thermocline setting, which reduces upwelling and nutrient advection (D'hondt et al., 2009; Lamy et al., 2014). This is reflected by low alkenones, *n*-alkanes and branched (br)GDGTs concentrations (Jaeschke et al., 2017). These factors likely lead to a seasonal bias if e.g., dust transport and macronutrient supply are increased in late spring to summer and relatively quickly exhausted.

4.3 GDGT – based (sub)surface temperatures

Similar to $U^{K'}_{37}$ values, isoGDGT-derived indices TEX^{H}_{86} and TEX^{L}_{86} increase along our transect from south to north. The values range from –0.48 to –0.61 (PS97/079) and from –0.39 to –0.53 (PS97/131) for TEX^{H}_{86} and TEX^{L}_{86}, respectively (cf. **Table A2**). In contrast to Coccolithophorids, *Thaumarchaeota* live at greater water depths (e.g., Karner et al., 2001) and occur also in the polar regions (e.g., Massana et al., 1998; Murray et al., 1998), which complicates the choice of an adequate temperature calibration, since reference data and sample sites for both characteristics remain scarce. For the isoGDGTs, we use six calibrations in total for both indices: the surface calibrations SST^{H}Kim, SST^{H}Kaiser and SST^{L}Kim, as well as the subsurface calibrations $Tsub^{H}$Kim, $Tsub^{H}$Kaiser and $Tsub^{L}$Kim (**Table A1**).

Surface and subsurface ranges for isoGDGTs are following the definition of Kaiser et al. (2015), Kim et al. (2012b) and Kim et al. (2012a), with a mean of 0 – 50 m water depth and 0 – 200 m water depth, respectively. We therefore used the WOA05-derived temperatures of depths from 10 m and 125 m for surface and subsurface, as they roughly correspond to the average values (**Figure 7**). Based on the surface calibrations, the temperatures range from ~11.5° C to 5° C for SST^{H}Kim, from ~9.5° C to 4° C for SST^{H}Kaiser, and from ~13° C to 6° C for SST^{L}Kim. With the subsurface calibrations, the temperatures range from ~9° C to 4° C for $Tsub^{H}$Kim, ~9° C to 5° C for $Tsub^{H}$Kaiser, and from ~10° C to 5° C for $Tsub^{L}$Kim (**Figure 7**).

The locations north of the SAF fit best to the modern WOA05-derived SSTs with the SST^{H}Kaiser calibration (**Figure 7B**) and appear to extend the surface regression line along the 5 – 10° C temperature range (**Figure 8A**). On average, the modern

Deleted: Table A2
Formatted: Font: Bold
Formatted: Font: Bold

Deleted: Table A1
Formatted: Font: Bold, English (US)
Formatted: English (US)
Formatted: Font: Bold, English (US)

temperatures are overestimated by ~1.3° C, which means they are no longer within the ±0.8° C standard error determined by Kaiser et al. (2015) for the surface calibration. In the subsurface, the $Tsub^H Kim$ and $Tsub^H Kaiser$ calibrations equally fit the modern WOA05-derived Tsub (**Figure 7D, E**), but the samples tend to fit better with the calibration line of $Tsub^H Kim$ (**Figure 8B**). On average, the modern WOA05-derived Tsub are overestimated here by ~1.6° C. Thus, the calculated temperatures are within the of ±2.2° C error range given by Kim et al. (2012a), but not within the ±0.6° C given by Kaiser et al. (2015) for the subsurface calibration. The samples from the DP instead do not fit to any calibration and overestimate modern WOA05-derived SSTs or Tsub in all calibrations, leading us to compare our results to other previously published data (see **Chapter 4.5**; **Figure 7** and **Figure 8**).

Apart from absolute temperature values, the slope of various calibrations allows to calculate relative temperature changes through time in marine sediment cores. Hence, the slope of the used temperature calibration in an area should adequately resemble the magnitude of relative temperature changes (e.g., between glacial and interglacial periods) to provide correct ΔT, which is e.g., often used in modelling studies (Burke et al., 2018), even if absolute temperature is offset. To determine which calibration best captures relative temperature changes in our study region, we compared our samples with published data from the Central South Pacific and New Zealand Margin (Ho et al., 2014; Jaeschke et al., 2017), in addition to the Northern – Central Chilean Margin (Kaiser et al., 2015) dataset (**Figure 9**). In **Figure 9A** – **D** we show in red the regressions of all sites located north of the SAF (called "local regression" hereafter) in comparison to the published six different SST and Tsub calibrations of Kim et al. (2010, 2012a and b), and Kaiser et al. (2015). In addition, we show the residuals in **Figure 9E, F** to illustrate which data are within the error range of the respective calibrations. For this purpose, the mean WOA05 values of 0 – 50 m and 0 – 200 m of the annual mean were subtracted from the respective temperature calibration.

Deleted: are

Deleted: both

The slope of the $SST^H Kim$ calibration shows a difference of ~3.2 to our local regression (**Figure 9A**), and yields best the relative temperature change across the region north of the SAF, although it generally yields the highest residuals (**Figure 9E**). The $Tsub^H Kim$ calibration, with a difference of ~3.9 between the two slopes (**Figure 9C**), captures the relative temperature changes as well. The latter corresponds to a temperature change (TEX^H_{86}: -0.2 to -0.3) of 5.5° C with $Tsub^H Kim$ and 5.1° C with our local regression. In contrast to $SST^H Kim$, the residuals are smaller and within the reported error range of ±2.2° C (Kim et al., 2012a) for most samples north of the SAF (**Figure 9F**). Again, the central South Pacific samples located south of the SAF significantly overestimate local SSTs or Tsub with annual residuals of ~8.4° C ($SST^H Kim$), ~6.6° C ($SST^H Kaiser$), ~8.1° C ($SST^L Kim$), ~6.4° C ($Tsub^H Kim$), ~6.9° C ($Tsub^H Kaiser$) and ~6.7° C ($Tsub^L Kim$).

Thus, our combined sample set north of the SAF fits the $Tsub^H Kim$ calibration best, while the samples south of the SAF do not match the commonly used calibrations, including the two calibrations based on TEX^L_{86} for (sub)polar regions (Kim et al., 2012b; Kim et al., 2010).

4.4 Influence of habitat depth and terrestrial input on *Thaumarchaeota*-derived temperatures

Habitat depth preferences for *Thaumarchaeota* and their response to seasonality (e.g., Schouten et al., 2013a) may influence the TEX^H_{86}-derived temperature signals. Since *Thaumarchaeota* are distributed throughout the entire water column, the decision to choose an optimal calibration is closely linked to an initial assumption about the water depth from which the signal originates (Karner et al., 2001). Hence, we applied the ratio of GDGT-2 to GDGT-3 (GDGT [2]/[3]) to locate the water depth of the temperature signal, since subsurface dwelling *Thaumarchaeota* preferentially yield GDGT-2 over the GDGT-3 (Kim et al., 2015; Taylor et al., 2013).

In the global ocean the distribution of *Thaumarchaeota* appears to vary within the water column and shows an increasing GDGT [2]/[3]-ratio with increasing depth (Dong et al., 2019; Hernández-Sánchez et al., 2014; Kim et al., 2015; Kim et al., 2016; Schouten et al., 2012; Taylor et al., 2013). Water column samples in the Arabian Sea and along the Portuguese margin show a GDGT [2]/[3]-ratio between <3.3 in the upper 50 m and 4.0 – 21.5 at >200 m water depth (Dong et al., 2019; Kim et al., 2016; Schouten et al., 2012). In the South China Sea, the GDGT [2]/[3]-ratio yields <3.5 at <100 m water depth and 5.9 – 8.6 at water depth >300 m (Dong et al., 2019). In the Southeast Atlantic, the GDGT [2]/[3]-ratio of between 0 – 50 m water depth is 1.9 – 3.4, 4.1 – 12.8 between 50 – 200 m water depth and 13 – 50 in water depth >200 m (Hernández-Sánchez et al., 2014). Thus, increasing GDGT [2]/[3]-ratios may not be strictly coupled to water depths across the world ocean. The GDGT [2]/[3]-ratio in the surface area seems similar in all regions with ~3.5, but subsurface values differ considerably. In the Southern Atlantic, the GDGT [2]/[3]-ratio increases to up to 12.8 within 50 – 200 m water depth, whereas at the Portuguese margin, the Arabian and the South China Sea, the GDGT [2]/[3]-ratio increases up to ~5.0, with oxygen content or nutrients being the most likely reason for such non-linearities (e.g., Basse et al., 2014; Villanueva et al., 2015).

The GDGT [2]/[3]–ratios in our extended study area vary between ~3 – 25. Values <5 (n = 7), indicating a surface signal, are found only occasionally off New Zealand and along the Chilean Margin. The majority of samples would correspond to a subsurface signal with a GDGT [2]/[3]–ratio >5, confirming our calibration choice (Tsub^{H}Kim) for the South Pacific. Studies from the Humboldt Current system, the Antarctic Peninsula and the North Pacific Gyre confirm this assumption and indicate a subsurface rather than a surface signal (Kalanetra et al., 2009; Karner et al., 2001; Massana et al., 1998; Quiñones et al., 2009). Here, we will distinguish between shallower subsurface (0 – 200 m water depth) and deep subsurface (>200 m water depth), to quantify the influence of deep subsurface-dwelling *Thaumarchaeota* to the GDGT distribution in the sediment. In general, it is assumed that a deep subsurface water influence is comparatively small, since *Thaumarchaeota* can be most effectively grazed, packed into fecal pellets, and transported to the seafloor within the photic zone (Wuchter et al., 2005). Nevertheless, variations in the GDGT [2]/[3]-ratio across the entire study area can provide information about regions that may be subject to a greater influence of deep subsurface dwelling *Thaumarchaeota*. Our South Pacific locations yield differences in GDGT [2]/[3]-ratio according to three principally differing boundary or forcing conditions: A hemipelagic continental margin setting, a deep thermocline oligotrophic gyre setting, and a SO frontal setting (**Figure 10**).

In the overall study area, our results suggest that isoGDGTs record shallower subsurface temperatures rather than surface temperatures. Samples along continental slopes tend to be less influenced by deep subsurface-dwelling *Thaumarchaeota*, while samples from the pelagic regions show a greater influence by deep subsurface-dwelling *Thaumarchaeota*. Samples along the Chilean Margin yield a mean GDGT [2]/[3]-ratio of ~6.2 to ~6.9, reflecting a transition between surface and shallow subsurface habitats. This is in line with Northern – Central Chilean Margin data, which show a positive correlation with both SSTs and

Tsub (Kaiser et al., 2015). The amount of deep subsurface-dwelling *Thaumarchaeota* increase with increasing distance from land, as shown by samples from the SW Pacific close to New Zealand. The GDGT [2]/[3]-ratios increase, in line with Taylor et al. (2013), from ~3.1 at ~600 m water depth to ~9.8 at >3000 m water depth to ~12.9 at >4000 m water depth (**Figure 10**). The highest influence of deep-dwelling *Thaumarchaeota* occurs in the South Pacific Gyre and in the eastern South Pacific, averaging a GDGT [2]/[3]-ratio of ~11.5 and indicating a potentially larger contribution of deep subsurface-dwelling *Thaumarchaeota* communities in the sediment, but no significant temperature deviations can be detected for the region north of the SAF (**Figure 9**). This suggests either that the influence of the deep subsurface-dwelling *Thaumarchaeota* on the temperature signal is smaller than previously thought, or that the distribution of the GDGT [2]/[3]-ratio in the subsurface in this region differs from that in the central South Pacific or continental margins.

Besides contributions from deeper living *Thaumarchaeota*, the GDGT [2]/[3]-ratio can also be influenced by isoGDGTs derived from terrestrial soils and peats, where the amount of the GDGT-3 is increased compared to the marine milieu (Weijers et al., 2006). This would result in GDGT [2]/[3]-ratio decreases with increasing terrestrial input, i.e., in the opposite direction of the influence of deeper living *Thaumarchaeota*. Therefore, we showed the GDGT [2]/[3]-ratios on a map with monthly average dust depositions (**Figure 12**) and found high GDGT [2]/[3]-ratios in areas with very little dust accumulation and lower GDGT [2]/[3]-ratios with higher dust accumulation, especially during march. This could explain the discrepancy between eastern and western pelagic South Pacific at a first glance and fit also to the low GDGT [2]/[3]-ratios along continental margins. To detect such distortions of terrigenous isoGDGTs on the GDGT [2]/[3]-ratio and therefore the TEX-based indices, the branched vs isoprenoid tetraether (BIT; should be <0.3) index was developed, where the brGDGTs occurring predominantly in terrestrial soils are related to the Crenarchaeol (Hopmans et al., 2004). The BIT is low (≤0.1) in this region, indicating no significant influence from land (Jaeschke et al., 2017; Kaiser et al., 2015). The visually good correlation between the GDGT [2]/[3]-ratios and the dust distribution indicates that future studies could potentially address more systematically underlying causes of these co-variations, at least in regions with low sedimentation rates but likely high eolian transport. Generally, however, isoGDGT-derived temperatures of samples north of the SAF fit quite well with Tsub^{H}Kim, so that both potential influences, deeper-dwelling *Thaumarchaeota* as well as terrigenous input seems to be negligible.

4.5 Towards an alternative southern hemisphere (sub)-polar calibration for isoGDGT-based temperatures

IsoGDGTs south of the SAF appear to have a lower sensitivity to temperature, which is in line with previous results, showing a large scatter of the TEX$_{86}$ – SST relationship in the polar regions (e.g., Kim et al., 2010; Fietz et al., 2020 and references therein). One reason given for the larger scatter may be a calibration based on satellite-assigned SSTs, which in polar regions yields values below the freezing point of seawater (Pearson and Ingalls, 2013). Consequently, a larger scatter of polar samples leads to a larger error of estimate in the related calibrations and would explain the occurrence of highest residuals with SST^{H}Kim and SST^{L}Kim in our study area in both north and south of the SAF (**Figure 7, 9**), i.e., where calibrations are based on satellite-assigned SSTs. However, our data does not show an increased scatter of values south of the SAF. Instead,

Deleted: compared

Deleted: nearly perfect fit

Deleted: of

Deleted: with

Deleted: should

Deleted: address

Deleted: potential

Deleted: Generally

they show a different TEX^H_{86} (TEX^L_{86}) – water temperature relationship, resulting in a lower slope of the calibration line (**Figure 9**).

We suspect that the SAF acts as a natural boundary, leading to differential responses within the *Thaumarchaeota* communities and their respective isoGDGTs to changing environmental parameters such as pH (Elling et al., 2015) or oxygen availability (Qin et al., 2015). Another reason for this pattern could be the increased occurrence of OH-isoGDGTs in polar regions. OH-isoGDGTs are present in lower amounts in the sediment than the isoGDGTs used in TEX^H_{86} and TEX^L_{86}, but are most abundant in higher latitudes (Fietz et al., 2013; Huguet et al., 2013; Liu et al., 2020). This increased occurrence of OH-isoGDGTs could indicate an adaptation to cold temperatures to maintain membrane fluidity. This could simultaneously affect the relationship of TEX-based indices to temperature, requiring a separate calibration for high latitudes. OH-isoGDGTs also show a stronger correlation with water temperature than isoGDGTs in both the Arctic (Fietz et al., 2013) and close to Antarctica (Liu et al., 2020), so another OH-isoGDGT-based index RI-OH' (= [OH-GDGT-1]+2*[OH-GDGT-2]/[OH-GDGT-0]+[OH-GDGT-1]+[OH-GDGT-2]; SST = (RI-OH'–0.1)/0.0382) has been proposed for polar regions (Lü et al., 2015). Moreover, OH-isoGDGTs were often not measured in legacy samples reported in early studies. Based on this, Fietz et al. (2020) recommended a multi-proxy approach for the polar regions, which includes both isoGDGTs and OH-isoGDGTs. However, isoGDGTs were more commonly used and OH-isoGDGTs may not be available for some data sets. A good example are the data sets (e.g.) $Tsub^L$Kim with n = 396 (Kim et al., 2012b) and RI-OH'-based surface calibration with n = 107 (Lü et al., 2015), which are designated for the same temperature range <15° C. A working TEX-based calibration specifically developed for the SO is therefore appropriate and may also be useful for further research on the functionality (OH)-isoGDGTs. Therefore, we here take an initial step and propose a modified TEX-based cold temperature calibration for the southern hemisphere (sub)polar region. We will then test the new calibration by (1) re-estimating the temperatures of a published sediment core and (2) comparing the SSTs and Tsub determined with the new calibration to RI-OH'-based SSTs.

This suggested calibration includes samples south of the SAF in the SO, and is extended by the data sets of Kim et al. (2010) and Lamping et al. (2021) with a total of n = 137 samples. Changes in TEX^H_{86} or general TEX_{86} indices below 5° C water temperature (according to SSTs south of the SAF in the Southern Ocean) are less pronounced than above 5° C, because of a weaker correlation of the isomer Cren' to water temperatures. Thus, it is excluded in the TEX^L_{86} – index as proposed by earlier studies (Kim et al., 2010). This is in line with our results, where all TEX^L_{86} calibrations show a stronger correlation than those based on TEX^H_{86} (*cf.* determination coefficient R^2; **Figure 11**). The maximum R^2 value of 0.7 (TEX^L_{86}, subsurface) is only slightly lower than previously published values (>0.8, *cf.*; **Table A1**), which is to be somewhat expected, because the scatter of both TEX^H_{86} and TEX^L_{86} indices below 5° C seems to be generally larger (Ho et al., 2014).

Based on our results, we propose a new TEX^L_{86} – based annual mean, subsurface (0 – 200 m) and surface (0 – 50 m) calibration for the Southern Ocean's polar and subpolar regions:

$$\text{Tsub} = 14.38 * TEX^L_{86} + 8.93, \quad (1)$$

Deleted: Table A1

Formatted: Font: Bold

Formatted: Font: Bold

$$\text{SST} = 10.71 * TEX_{86}^{L} + 6.64, \quad (2)$$

The standard error of ±0.6° C (±0.5° C) for our subsurface (surface) calibration is lower than the standard error from the previous subsurface (surface) calibration $Tsub^L$Kim (SST^LKim) with ±2.8° C (±4° C), which is probably due to the latter's lower data density. With this new calibration, just 44 (40) of the 137 samples lie outside this error range. Another major difference between our calibration and $Tsub^L$Kim (SST^LKim) is the slope of the regression line being much flatter here at 14.4 (10.7) than the slope of the calibration $Tsub^L$Kim (SST^LKim) with 50.8 (67.5) (**Figure 9**). This leads to a generally smaller temperature increase with an increasing TEX^L_{86} index. An increase of TEX^L_{86} from -0.6 to -0.5 e.g., corresponds to a temperature change of 1.4° C in our subsurface calibration and of 5.1° C in $Tsub^L$Kim.

(1) Using our new calibration, we compare recalculated results with the previously used subsurface TEX^L_{86} calibration $Tsub^L$Kim (**Figure 13**) on core MD03-2601 (66°03.07' S, 138°33.43' E; Kim et al., 2012b) from the eastern Indian sector of the SO covering the Holocene, where the authors acknowledged that a temperature offset existed, but within the specified calibration error range of ±2.8° C. Temperatures based on our subsurface calibration are on average ~2.5° C colder than the ones based on the previously used subsurface calibration $Tsub^L$Kim. With our new calibration, temperatures remain relatively constant at -0.8° C, and at 1.5° C with the subsurface calibration $Tsub^L$Kim between 4.8 – 3.1 ka BP. Modern temperatures near the core site agree well with core top results from our new calibration with -0.7° C (65.5° S, 138.5° E; Locarnini et al., 2006) vs. -0.8° C (our reconstruction) for the subsurface layer. The recalculated temperature increases, associated with warmer nutrient-rich modified Circumpolar Deep-Water intrusions, show an attenuated amplitude with the new calibration (**Figure 13**). The amplitude based on our new calibration is 1.2° C around 1.7 ka BP, whereas it is 4.2° C with the original subsurface calibration $Tsub^L$Kim and therefore better fits to the expected temperatures.

(2) While we do not have OH-isoGDGTs for the Kim et al. (2010), Jaeschke et al. (2017) and Ho et al. (2012) datasets, we calculated SSTs based on the RI-OH' index and compared them to SSTs and Tsub based on our calibrations for all samples south of the SAF for which OH-isoGDGTs are available (Drake Passage, Antarctic Peninsula, Weddell Sea and Amundsen Sea). The results of all three calibrations (TEX^L_{86}-based SST and Tsub; RI-OH'-based SST) fit (**Figure 14**), with a temperature discrepancy of ±1° C from each other. One exception here is the Drake Passage, where the RI-OH'-based SSTs show residuals of >2° C. Considering the standard error of ±6° C (Lü et al., 2015), all RI-OH'-based SSTs are within this error range. The upper ocean temperatures in the Drake Passage are the only ones in this area above zero, which may explain the larger residuals of the RI-OH'-based SSTs. It is possible that similar to the subsurface calibration of Kim et al. (2012b), the relative temperature change is not correctly captured due to a too steep regression line for samples south of the SAF. The calibration of Lü et al. (2015) includes only a few samples from higher latitudes, most of them from the Arctic, and samples in the temperature range between 1 – 3° C are almost absence. A RI-OH'-based calibration for samples south of the SAF could increase the sensitivity of the proxy and decrease the standard error, similar to the TEX^L_{86}-index demonstrated here. This is in contrast to the good agreement of the remaining samples, both with our TEX-based temperature reconstructions and with the WOA05-derived

temperatures. A calibration based on TEX^L_{86} developed specifically for the SO yields comparable results to a calibration based on OH-isoGDGTs. We agree with Fietz et al. (2020) to determine both indices, if possible, as this is a good way to check the consistency of temperature reconstructions.

5 Conclusion

In this study, we provide a qualitative evaluation of the most common temperature calibrations for alkenones and isoGDGTs in the South Pacific and potential environmental influencing factors. For alkenone-derived SSTs, our results provide a best fit with the global core-top calibration of Müller et al. (1998). On a regional scale, the Southern Chilean Margin and the Drake Passage show a small seasonal effect of ~1° C towards warmer SSTs south of ~50° S, albeit well within the ±1.5° C standard error for alkenone derived SSTs (Müller et al., 1998). Excluding local influences, the seasonal effect in the DP is slightly higher at about ~2° C and no longer within the error range of calibration by Müller et al. (1998). In contrast, the samples from the Central Southern Pacific Ocean show no clear seasonal trend. Causes for this difference between the two areas are increased seasonal provision of nutrients, or more pronounced stratification at the sites proximal to continental runoff along the Chilean margin during late summer time.

IsoGDGT-based temperatures show a more complex pattern, which necessitates choosing the temperature calibration carefully, depending on the area. The optimal calibration for isoGDGT-based temperature reconstructions in the South Pacific is the subsurface calibration Tsub (Kim et al., 2012a), for samples north of the Sub-Antarctic Front, in line with evidence from compiled GDGT [2]/[3]-ratios, which indicate a subsurface of 0 to 200 m water depth, rather than surface habitat depth throughout the study area. South of the Sub-Antarctic Front, all existing calibrations overestimate local WOA05-derived temperatures. Furthermore, the GDGT [2]/[3]-ratios do also correlate with the average monthly dust deposition in the South Pacific. A new calibration for subpolar and polar areas yields lower absolute subsurface temperatures, as well as lower relative changes within the commonly accepted standard error range. The results of this new calibration fit well within the standard error with OH-GDGT-derived temperatures.

For future work, we recommend to extend both the geographical area coverage in subpolar and polar regions and the sample density. Furthermore, the influence of seasonality and habitat should be investigated to assess how strongly these factors affect paleo-temperature reconstructions.

Appendix A

Table A1: Common indices and their most important temperature calibrations for alkenones and isoGDGTs, with their determination coefficients (R^2) and abbreviations used in this paper. $U^{K'}_{37}$ = Alkenone unsaturation index consisting of 37 carbon atoms; TEX_{86} = Tetraether index consisting of 86 carbon atoms; TEX^H_{86} = Tetraether index for water temperatures above 15° C; TEX^L_{86} = Tetraether index for water temperatures below 15° C; SST = Sea Surface Temperature; Tsub = Sea subsurface temperatures (0 – 200 m water depth). Abbreviation: the here defined abbreviations will be used in the main text.

	Equation	R^2	Abbreviation	References
1	$U^{K'}_{37} = [C_{37:2}] / [C_{37:2}] + [C_{37:3}]$			Prahl and Wakeham (1987)
2	$SST = (U^{K'}_{37} - 0.043) / 0.033$	0.994		Prahl and Wakeham (1987)
3	$SST = (U^{K'}_{37} - 0.039) / 0.034$	0.994	Prahl88	Prahl et al. (1988)
4	$SST = (U^{K'}_{37} - 0.044) / 0.033$	0.958	Müller98	Müller et al. (1998)
5	$SST = (U^{K'}_{37} + 0.082) / 0.038$	0.921	Sikes97	Sikes et al. (1997)
6	$TEX_{86} = \frac{[2] + [3] + [Cren']}{[1] + [2] + [3] + [Cren']}$			Schouten et al. (2002)
7	$TEX^{H}_{86} = log \frac{[2] + [3] + [Cren']}{[1] + [2] + [3] + [Cren']}$			Kim et al. (2010)
8	$TEX^{L}_{86} = log \frac{[2]}{[1] + [2] + [3]}$			Kim et al. (2010)
9	$SST = 68.4 * TEX^{H}_{86} + 38.6$	0.87	$SST^{H}Kim$	Kim et al. (2010)
10	$Tsub = 54.7 * TEX^{H}_{86} + 30.7$	0.84	$Tsub^{H}Kim$	Kim et al. (2012a)
11	$SST = 59.6 * TEX^{H}_{86} + 33$	0.91	$SST^{H}Kaiser$	Kaiser et al. (2015)
12	$Tsub = 32.1 * TEX^{H}_{86} + 21.5$	0.86	$Tsub^{H}Kaiser$	Kaiser et al. (2015)
13	$SST = 67.5 * TEX^{L}_{86} + 46.9$	0.86	$SST^{L}Kim$	Kim et al. (2010)
14	$Tsub = 50.8 * TEX^{L}_{86} + 36.1$	0.87	$Tsub^{L}Kim$	Kim et al. (2012b)

Table A2: Surface sediment sample results of this study. $U^{K'}_{37}$ = Alkenone unsaturation index consisting of 37 carbon atoms; TEX_{86} = Tetraether index consisting of 86 carbon atoms; TEX^{H}_{86} = Tetraether index for water temperatures above 15° C; TEX^{L}_{86} = Tetraether index for water temperatures below 15° C.

	Station	Latitude	Longitude	Depth [m]	$U^{K'}_{37}$	TEX^{H}_{86}	TEX^{L}_{86}
	Southern Chilean Margin						
1	PS97/139-1	52° 26.56' S	75° 42.42' W	640	0.40	-0.40	-0.58
2	PS97/134-1	52° 40.97' S	75° 34.85' W	1075.1	0.36	-0.39	-0.54
3	PS97/132-2	52° 37.01' S	75° 35.14' W	843	0.38	-0.47	-0.60
4	PS97/131-1	52° 39.58' S	75° 33.97' W	1028.2	0.35	-0.39	-0.53
5	PS97/129-2	53° 19.28' S	75° 12.84' W	1879.4	0.34	-0.41	-0.54
6	PS97/128-1	53° 38.04' S	75° 32.71' W	2293.7	0.32	-0.42	-0.54
7	PS97/122-2	54° 5.85' S	74° 54.89' W	2560	0.31	-0.41	-0.53
8	PS97/114-1	54° 34.68' S	76° 38.85' W	3863	0.26	-0.41	-0.50
9	PS97/027-1	54° 23.05' S	74° 36.30' W	2349.2	0.28	-0.41	-0.53
10	PS97/024-2	54° 35.27' S	73° 57.30' W	1272.8	-	-	-
11	PS97/022-1	54° 42.03' S	73° 48.38' W	1615.1	0.27	-0.41	-0.55
12	PS97/021-1	55° 6.91' S	72° 40.09' W	1840.4	0.30	-0.41	-0.54
13	PS97/020-1	55° 30.80' S	71° 38.22' W	2104.3	0.27	-0.42	-0.54
14	PS97/015-2	55° 43.89' S	70° 53.55' W	1886.3	0.31	-0.42	-0.55
15	PS97/094-1	57° 0.17' S	70° 58.32' W	3993.4	0.31	-0.39	-0.52
16	PS97/093-3	57° 29.92' S	70° 16.57' W	3782.2	0.36	-0.42	-0.54
17	PS97/097-1	57° 3.27' S	67° 4.00' W	2318.6	0.30	-0.42	-0.53
18	PS97/096-1	56° 4.53' S	66° 8.96' W	1620.7	0.31	-0.44	-0.55
19	PS97/095-1	56° 14.68' S	66° 14.95' W	1652.1	0.25	-0.43	-0.55
	Drake Passage Shackleton Fracture Zone						
20	PS97/089-2	58° 13.60' S	62° 43.63' W	3431.9	0.18	-0.43	-0.56
21	PS97/086-2	58° 38.65' S	61° 23.82' W	2968.9	0.15	-0.45	-0.56

22	PS97/085-2	58° 21.28' S	62° 10.07' W	3090.7	0.16	-0.43	-0.55
23*	PS97/084-2	58° 52.14' S	60° 51.91' W	3617.4	0.10	-0.46	-0.58
24*	PS97/083-1	58° 59.65' S	60° 34.28' W	3756.3	0.12	-0.49	-0.60
25*	PS97/080-2	59° 40.49' S	59° 37.86' W	3112.7	0.12	-0.46	-0.56
26*	PS97/079-1	60° 8.55' S	58° 59.42' W	3539.3	0.07	-0.48	-0.61
	Drake Passage Phoenix Antarctic Ridge						
27*	PS97/042-1	59° 50.62' S	66° 5.77' W	4172	0.12	-0.43	-0.54
28*	PS97/044-1	60° 36.80' S	66° 1.34' W	1202.8	-	-0.48	-0.57
29*	PS97/045-1	60° 34.27' S	66° 5.67' W	2292	0.14	-0.47	-0.55
30*	PS97/046-6	60° 59.74' S	65° 21.40' W	2802.7	0.13	-0.45	-0.56
31*	PS97/048-1	61° 26.40' S	64° 53.27' W	3455.2	0.14	-0.42	-0.55
32*	PS97/049-2	61° 40.28' S	64° 57.74' W	3752.2	0.14	-0.47	-0.58
33*	PS97/052-3	62° 29.93' S	64° 17.63' W	2889.8	-	-0.46	-0.60

* isoGDGTs Lamping et al. (2021); Alkenone *this study*

Data availability. All locations and the three main indices of the new 33 samples of this study are available in **Table A2**.

Author contributions. The study was conceived by JRH and LL-J; MEV, JRH, JH and NR contributed with analytical tools; JRH, LL-J, JK, AJ analyzed data; JRH drafted the paper and figures; LL-J supervised the study. All authors contributed to the interpretation and discussion of the results as well as commented on, or contributed to the draft and final version of the manuscript.

Acknowledgements. We thank master and crew of R/V Polarstern, as well as the science party for their professional support on expedition PS97 "Paleo-Drake". We thank Sophie Ehrhardt for providing unpublished alkenone data. We thank the technicians Walter Luttmer and Denise Diekstall for their support in the laboratory. We acknowledge funding through the AWI institutional research programs "PACES-II" and "Changing Earth – Sustaining our Future", as well as through the REKLIM initiative. We acknowledge the use of imagery from the NASA Worldview application (https://worldview.earthdata.nasa.gov/), part of the NASA Earth Observing System Data and Information System (EOSDIS). We thank the two anonymous reviewers and the editor for their constructive, detailed, and very helpful comments, which allowed us to improve our work significantly.

Financial support. This research has been supported by the AWI institutional research programs “PACES-II” and “Changing Earth – Sustaining our Future”, as well as through the REKLIM initiative.

Competing Interests. The authors declare no conflict of interest.

References

Basse, A., Zhu, C., Versteegh, G. J. M., Fischer, G., Hinrichs, K. U., and Mollenhauer, G.: Distribution of intact and core tetraether lipids in water column profiles of suspended particulate matter off Cape Blanc, NW Africa, Organic Geochemistry, 72, 1-13, 10.1016/j.orggeochem.2014.04.007, 2014.

Baumann, K.-H., Andruleit, H., Böckel, B., Geisen, M., and Kinkel, H.: The significance of extant coccolithophores as indicators of ocean water masses, surface water temperature, and palaeoproductivity: a review, Paläontologische Zeitschrift, 79, 93-112, 10.1007/bf03021756, 2005.

Belt, S. T., Brown, T. A., Ampel, L., Cabedo-Sanz, P., Fahl, K., Kocis, J. J., Massé, G., Navarro-Rodriguez, A., Ruan, J., and Xu, Y.: An inter-laboratory investigation of the Arctic sea ice biomarker proxy IP₂₅ in marine sediments: key outcomes and recommendations, Climate of the Past, 10, 155-166, 10.5194/cp-10-155-2014, 2014.

Brassell, S. C., Eglinton, G., Marlowe, I. T., Pflaumann, U., and Sarnthein, M.: Molecular Stratigraphy - a New Tool for Climatic Assessment, Nature, 320, 129-133, 10.1038/320129a0, 1986.

Brochier-Armanet, C., Boussau, B., Gribaldo, S., and Forterre, P.: Mesophilic Crenarchaeota: proposal for a third archaeal phylum, the Thaumarchaeota, Nat Rev Microbiol, 6, 245-252, 10.1038/nrmicro1852, 2008.

Burke, K. D., Williams, J. W., Chandler, M. A., Haywood, A. M., Lunt, D. J., and Otto-Bliesner, B. L.: Pliocene and Eocene provide best analogs for near-future climates, Proc Natl Acad Sci U S A, 115, 13288-13293, 10.1073/pnas.1809600115, 2018.

Caniupán, M., Lamy, F., Lange, C. B., Kaiser, J., Kilian, R., Arz, H. W., León, T., Mollenhauer, G., Sandoval, S., De Pol-Holz, R., Pantoja, S., Wellner, J., and Tiedemann, R.: Holocene sea-surface temperature variability in the Chilean fjord region, Quaternary Research, 82, 342-353, 10.1016/j.yqres.2014.07.009, 2014.

Chong, P. L.: Archaebacterial bipolar tetraether lipids: Physico-chemical and membrane properties, Chem Phys Lipids, 163, 253-265, 10.1016/j.chemphyslip.2009.12.006, 2010.

Conte, M. H., Sicre, M.-A., Rühlemann, C., Weber, J. C., Schulte, S., Schulz-Bull, D., and Blanz, T.: Global temperature calibration of the alkenone unsaturation index (UK′37) in surface waters and comparison with surface sediments, Geochemistry, Geophysics, Geosystems, 7, 10.1029/2005gc001054, 2006.

D'Hondt, S., Spivack, A. J., Pockalny, R., Ferdelman, T. G., Fischer, J. P., Kallmeyer, J., Abrams, L. J., Smith, D. C., Graham, D., Hasiuk, F., Schrum, H., and Stancin, A. M.: Subseafloor sedimentary life in the South Pacific Gyre, Proc Natl Acad Sci U S A, 106, 11651-11656, 10.1073/pnas.0811793106, 2009.

Dávila, P. M., Figueroa, D., and Müller, E.: Freshwater input into the coastal ocean and its relation with the salinity distribution off austral Chile (35–55°S), Continental Shelf Research, 22, 521-534, 10.1016/s0278-4343(01)00072-3, 2002.

Dong, L., Li, Z. Y., and Jia, G. D.: Archaeal ammonia oxidation plays a part in late Quaternary nitrogen cycling in the South China Sea, Earth and Planetary Science Letters, 509, 38-46, 10.1016/j.epsl.2018.12.023, 2019.

Durak, G. M., Taylor, A. R., Walker, C. E., Probert, I., de Vargas, C., Audic, S., Schroeder, D., Brownlee, C., and Wheeler, G. L.: A role for diatom-like silicon transporters in calcifying coccolithophores, Nat Commun, 7, 10543, 10.1038/ncomms10543, 2016.

Elling, F. J., Konneke, M., Mussmann, M., Greve, A., and Hinrichs, K. U.: Influence of temperature, pH, and salinity on membrane lipid composition and TEX86 of marine planktonic thaumarchaeal isolates, Geochimica Et Cosmochimica Acta, 171, 238-255, 10.1016/j.gca.2015.09.004, 2015.

Epstein, B. L., D'Hondt, S., and Hargraves, P. E.: The possible metabolic role of C37 alkenones in Emiliania huxleyi, Organic Geochemistry, 32, 867-875, 10.1016/s0146-6380(01)00026-2, 2001.

Fietz, S., Ho, S. L., and Huguet, C.: Archaeal Membrane Lipid-Based Paleothermometry for Applications in Polar Oceans, Oceanography, 33, 104-114, 10.5670/oceanog.2020.207, 2020.

Fietz, S., Ho, S. L., Huguet, C., Rosell-Mele, A., and Martinez-Garcia, A.: Appraising GDGT-based seawater temperature indices in the Southern Ocean, Organic Geochemistry, 102, 93-105, 10.1016/j.orggeochem.2016.10.003, 2016.

Fietz, S., Huguet, C., Rueda, G., Hambach, B., and Rosell-Mele, A.: Hydroxylated isoprenoidal GDGTs in the Nordic Seas, Marine Chemistry, 152, 1-10, 10.1016/j.marchem.2013.02.007, 2013.

Gabriel, J. L. and Chong, P. L.: Molecular modeling of archaebacterial bipolar tetraether lipid membranes, Chem Phys Lipids, 105, 193-200, 10.1016/s0009-3084(00)00126-2, 2000.
Garreaud, R., Lopez, P., Minvielle, M., and Rojas, M.: Large-Scale Control on the Patagonian Climate, Journal of Climate, 26, 215-230, 10.1175/Jcli-D-12-00001.1, 2013.
Global_Modeling_and_Assimilation_Office_(GAMO): MERRA-2 tavgM_2d_adg_Nx: 2d,Monthly mean,Time-averaged,Single-Level,Assimilation,Aerosol Diagnostics (extended) V5.12.4 [dataset], 10.5067/RZIK2TV7PP38, 2015.
Herbert, T. D.: Review of alkenone calibrations (culture, water column, and sediments), Geochemistry Geophysics Geosystems, 2, 10.1029/2000gc000055, 2001.
Herbert, T. D.: Alkenone Paleotemperature Determinations, in: Treatise on Geochemistry, 399-433, 10.1016/b978-0-08-095975-7.00615-x, 2014.
Herbert, T. D., Peterson, L. C., Lawrence, K. T., and Liu, Z.: Tropical ocean temperatures over the past 3.5 million years, Science, 328, 1530-1534, 10.1126/science.1185435, 2010.
Hernández-Sánchez, M. T., Woodward, E. M. S., Taylor, K. W. R., Henderson, G. M., and Pancost, R. D.: Variations in GDGT distributions through the water column in the South East Atlantic Ocean, Geochimica et Cosmochimica Acta, 132, 337-348, 10.1016/j.gca.2014.02.009, 2014.
Ho, S. L., Mollenhauer, G., Lamy, F., Martinez-Garcia, A., Mohtadi, M., Gersonde, R., Hebbeln, D., Nunez-Ricardo, S., Rosell-Mele, A., and Tiedemann, R.: Sea surface temperature variability in the Pacific sector of the Southern Ocean over the past 700 kyr, Paleoceanography, 27, 10.1029/2012pa002317, 2012.
Ho, S. L., Mollenhauer, G., Fietz, S., Martinez-Garcia, A., Lamy, F., Rueda, G., Schipper, K., Meheust, M., Rosell-Mele, A., Stein, R., and Tiedemann, R.: Appraisal of TEX86 and TEX86L thermometries in subpolar and polar regions, Geochimica Et Cosmochimica Acta, 131, 213-226, 10.1016/j.gca.2014.01.001, 2014.
Hopmans, E. C., Schouten, S., and Damste, J. S. S.: The effect of improved chromatography on GDGT-based palaeoproxies, Organic Geochemistry, 93, 1-6, 10.1016/j.orggeochem.2015.12.006, 2016.
Hopmans, E. C., Weijers, J. W. H., Schefuss, E., Herfort, L., Damste, J. S. S., and Schouten, S.: A novel proxy for terrestrial organic matter in sediments based on branched and isoprenoid tetraether lipids, Earth and Planetary Science Letters, 224, 107-116, 10.1016/j.epsl.2004.05.012, 2004.
Huguet, C., Fietz, S., and Rosell-Mele, A.: Global distribution patterns of hydroxy glycerol dialkyl glycerol tetraethers, Organic Geochemistry, 57, 107-118, 10.1016/j.orggeochem.2013.01.010, 2013.
Jaeschke, A., Wengler, M., Hefter, J., Ronge, T. A., Geibert, W., Mollenhauer, G., Gersonde, R., and Lamy, F.: A biomarker perspective on dust, productivity, and sea surface temperature in the Pacific sector of the Southern Ocean, Geochimica Et Cosmochimica Acta, 204, 120-139, 10.1016/j.gca.2017.01.045, 2017.
Kaiser, J., Schouten, S., Kilian, R., Arz, H. W., Lamy, F., and Damste, J. S. S.: Isoprenoid and branched GDGT-based proxies for surface sediments from marine, fjord and lake environments in Chile, Organic Geochemistry, 89-90, 117-127, 10.1016/j.orggeochem.2015.10.007, 2015.
Kalanetra, K. M., Bano, N., and Hollibaugh, J. T.: Ammonia-oxidizing Archaea in the Arctic Ocean and Antarctic coastal waters, Environ Microbiol, 11, 2434-2445, 10.1111/j.1462-2920.2009.01974.x, 2009.
Karner, M. B., DeLong, E. F., and Karl, D. M.: Archaeal dominance in the mesopelagic zone of the Pacific Ocean, Nature, 409, 507-510, 10.1038/35054051, 2001.
Kim, J. H., Villanueva, L., Zell, C., and Damste, J. S. S.: Biological source and provenance of deep-water derived isoprenoid tetraether lipids along the Portuguese continental margin, Geochimica Et Cosmochimica Acta, 172, 177-204, 10.1016/j.gca.2015.09.010, 2016.
Kim, J. H., Romero, O. E., Lohmann, G., Donner, B., Laepple, T., Haam, E., and Damste, J. S. S.: Pronounced subsurface cooling of North Atlantic waters off Northwest Africa during Dansgaard-Oeschger interstadials, Earth and Planetary Science Letters, 339, 95-102, 10.1016/j.epsl.2012.05.018, 2012a.
Kim, J. H., Crosta, X., Willmott, V., Renssen, H., Bonnin, J., Helmke, P., Schouten, S., and Damste, J. S. S.: Holocene subsurface temperature variability in the eastern Antarctic continental margin, Geophysical Research Letters, 39, 10.1029/2012gl051157, 2012b.
Kim, J. H., van der Meer, J., Schouten, S., Helmke, P., Willmott, V., Sangiorgi, F., Koc, N., Hopmans, E. C., and Damste, J. S. S.: New indices and calibrations derived from the distribution of crenarchaeal isoprenoid tetraether lipids: Implications for past sea surface temperature reconstructions, Geochimica Et Cosmochimica Acta, 74, 4639-4654, 10.1016/j.gca.2010.05.027, 2010.
Kim, J. H., Schouten, S., Rodrigo-Gamiz, M., Rampen, S., Marino, G., Huguet, C., Helmke, P., Buscail, R., Hopmans, E. C., Pross, J., Sangiorgi, F., Middelburg, J. B. M., and Damste, J. S. S.: Influence of deep-water derived isoprenoid tetraether lipids on the TEX86H paleothermometer in the Mediterranean Sea, Geochimica Et Cosmochimica Acta, 150, 125-141, 10.1016/j.gca.2014.11.017, 2015.
Koenig, Z., Provost, C., Ferrari, R., Sennechael, N., and Rio, M. H.: Volume transport of the Antarctic Circumpolar Current: Production and validation of a 20 year long time series obtained from in situ and satellite observations, Journal of Geophysical Research-Oceans, 119, 5407-5433, 10.1002/2014jc009966, 2014.

Lamping, N., Muller, J., Hefter, J., Mollenhauer, G., Haas, C., Shi, X. X., Vorrath, M. E., Lohmann, G., and Hillenbrand, C. D.: Evaluation of lipid biomarkers as proxies for sea ice and ocean temperatures along the Antarctic continental margin, Climate of the Past, 17, 2305-2326, 10.5194/cp-17-2305-2021, 2021.

Lamy, F.: The Expedition PS97 of the Research Vessel POLARSTERN to the Drake Passage in 2016 , Berichte zur Polar- und Meeresforschung = Reports on polar and marine research, Bremerhaven, Alfred Wegener Institute for Polar and Marine Research, 571 p., http://doi.org/10.2312/BzPM_0701_2016, 2016.

Lamy, F., Kilian, R., Arz, H. W., Francois, J. P., Kaiser, J., Prange, M., and Steinke, T.: Holocene changes in the position and intensity of the southern westerly wind belt, Nature Geoscience, 3, 695-699, 10.1038/Ngeo959, 2010.

Lamy, F., Gersonde, R., Winckler, G., Esper, O., Jaeschke, A., Kuhn, G., Ullermann, J., Martinez-Garcia, A., Lambert, F., and Kilian, R.: Increased dust deposition in the Pacific Southern Ocean during glacial periods, Science, 343, 403-407, 10.1126/science.1245424, 2014.

Liu, R. J., Han, Z. B., Zhao, J., Zhang, H. F., Li, D., Ren, J. Y., Pan, J. M., and Zhang, H. S.: Distribution and source of glycerol dialkyl glycerol tetraethers (GDGTs) and the applicability of GDGT-based temperature proxies in surface sediments of Prydz Bay, East Antarctica, Polar Research, 39, 10.33265/polar.v39.3557, 2020.

Locarnini, R. A., Mishonov, A. V., Antonov, J. I., Boyer, T. P., and Garcia, H. E.: World Ocean Atlas 2005, Volume 1: Temperature, S. Levitus, Ed. NOAA Atlas NESDIS 61 [dataset], 2006.

Locarnini, R. A., Mishonov, A. V., Antonov, J. I., Boyer, T. P., Garcia, H. E., Baranova, O. K., Zweng, M. M., and Johnson, D. R.: World Ocean Atlas 2009, Volume 1: Temperature S. Levitus, Ed., NOAA Atlas NESIDIS 68, U.S. Government Printing Office, Washington, D.C., 184 pp., 2010.

Lü, X., Liu, X.-L., Elling, F. J., Yang, H., Xie, S., Song, J., Li, X., Yuan, H., Li, N., and Hinrichs, K.-U.: Hydroxylated isoprenoid GDGTs in Chinese coastal seas and their potential as a paleotemperature proxy for mid-to-low latitude marginal seas, Organic Geochemistry, 89-90, 31-43, 10.1016/j.orggeochem.2015.10.004, 2015.

Massana, R., Taylor, L. J., Murray, A. E., Wu, K. Y., Jeffrey, W. H., and DeLong, E. F.: Vertical distribution and temporal variation of marine planktonic archaea in the Gerlache Strait, Antarctica, during early spring, Limnology and Oceanography, 43, 607-617, 10.4319/lo.1998.43.4.0607, 1998.

Max, L., Lembke-Jene, L., Zou, J., Shi, X., and Tiedemann, R.: Evaluation of reconstructed sea surface temperatures based on U37k′ from sediment surface samples of the North Pacific, Quaternary Science Reviews, 243, 10.1016/j.quascirev.2020.106496, 2020.

Méheust, M., Fahl, K., and Stein, R.: Variability in modern sea surface temperature, sea ice and terrigenous input in the sub-polar North Pacific and Bering Sea: Reconstruction from biomarker data, Organic Geochemistry, 57, 54-64, 10.1016/j.orggeochem.2013.01.008, 2013.

Müller, P. J., Kirst, G., Ruhland, G., von Storch, I., and Rosell-Melé, A.: Calibration of the alkenone paleotemperature index U37K′ based on core-tops from the eastern South Atlantic and the global ocean (60°N-60°S), Geochimica et Cosmochimica Acta, 62, 1757-1772, 10.1016/s0016-7037(98)00097-0, 1998.

Murray, A. E., Preston, C. M., Massana, R., Taylor, L. T., Blakis, A., Wu, K., and DeLong, E. F.: Seasonal and spatial variability of bacterial and archaeal assemblages in the coastal waters near Anvers Island, Antarctica, Appl Environ Microbiol, 64, 2585-2595, 10.1128/AEM.64.7.2585-2595.1998, 1998.

Orsi, A. H., Whitworth, T., and Nowlin, W. D.: On the Meridional Extent and Fronts of the Antarctic Circumpolar Current, Deep-Sea Research Part I-Oceanographic Research Papers, 42, 641-673, 10.1016/0967-0637(95)00021-W, 1995.

Pearson, A. and Ingalls, A. E.: Assessing the Use of Archaeal Lipids as Marine Environmental Proxies, Annual Review of Earth and Planetary Sciences, Vol 41, 41, 359-384, 10.1146/annurev-earth-050212-123947, 2013.

Popp, B. N., Kenig, F., Wakeham, S. G., Laws, E. A., and Bidigare, R. R.: Does growth rate affect ketone unsaturation and intracellular carbon isotopic variability inEmiliania huxleyi?, Paleoceanography, 13, 35-41, 10.1029/97pa02594, 1998.

Prahl, F. G. and Wakeham, S. G.: Calibration of unsaturation patterns in long-chain ketone compositions for palaeotemperature assessment, Nature, 330, 367-369, 10.1038/330367a0, 1987.

Prahl, F. G., Mix, A. C., and Sparrow, M. A.: Alkenone paleothermometry: Biological lessons from marine sediment records off western South America, Geochimica Et Cosmochimica Acta, 70, 101-117, 10.1016/j.gca.2005.08.023, 2006.

Prahl, F. G., Muehlhausen, L. A., and Zahnle, D. L.: Further Evaluation of Long-Chain Alkenones as Indicators of Paleoceanographic Conditions, Geochimica Et Cosmochimica Acta, 52, 2303-2310, 10.1016/0016-7037(88)90132-9, 1988.

Prahl, F. G., Rontani, J. F., Zabeti, N., Walinsky, S. E., and Sparrow, M. A.: Systematic pattern in U-37(K ') - Temperature residuals for surface sediments from high latitude and other oceanographic settings, Geochimica Et Cosmochimica Acta, 74, 131-143, 10.1016/j.gca.2009.09.027, 2010.

Qin, W., Carlson, L. T., Armbrust, E. V., Devol, A. H., Moffett, J. W., Stahl, D. A., and Ingalls, A. E.: Confounding effects of oxygen and temperature on the TEX86 signature of marine Thaumarchaeota, Proc Natl Acad Sci U S A, 112, 10979-10984, 10.1073/pnas.1501568112, 2015.

Quiñones, R. A., Levipan, H. A., and Urrutia, H.: Spatial and temporal variability of planktonic archaeal abundance in the Humboldt Current System off Chile, Deep Sea Research Part II: Topical Studies in Oceanography, 56, 1073-1082, 10.1016/j.dsr2.2008.09.012, 2009.

Field Code Changed

Rintoul, S. R.: The global influence of localized dynamics in the Southern Ocean, Nature, 558, 209-218, 10.1038/s41586-018-0182-3, 2018.
Saavedra-Pellitero, M., Baumann, K. H., Flores, J. A., and Gersonde, R.: Biogeographic distribution of living coccolithophores in the Pacific sector of the Southern Ocean, Marine Micropaleontology, 109, 1-20, 10.1016/j.marmicro.2014.03.003, 2014.
Saavedra-Pellitero, M., Baumann, K. H., Fuertes, M. A., Schulz, H., Marcon, Y., Vollmar, N. M., Flores, J. A., and Lamy, F.: Calcification and latitudinal distribution of extant coccolithophores across the Drake Passage during late austral summer 2016, Biogeosciences, 16, 3679-3702, 10.5194/bg-16-3679-2019, 2019.
Schneider, C., Glaser, M., Kilian, R., Santana, A., Butorovic, N., and Casassa, G.: Weather Observations Across the Southern Andes at 53°S, Physical Geography, 24, 97-119, 10.2747/0272-3646.24.2.97, 2003.
Schouten, S., Hopmans, E. C., and Damste, J. S. S.: The organic geochemistry of glycerol dialkyl glycerol tetraether lipids: A review, Organic Geochemistry, 54, 19-61, 10.1016/j.orggeochem.2012.09.006, 2013a.
Schouten, S., Hopmans, E. C., Schefuß, E., and Sinninghe Damsté, J. S.: Distributional variations in marine crenarchaeotal membrane lipids: a new tool for reconstructing ancient sea water temperatures?, Earth and Planetary Science Letters, 204, 265-274, 10.1016/s0012-821x(02)00979-2, 2002.
Schouten, S., Huguet, C., Hopmans, E. C., Kienhuis, M. V., and Damste, J. S.: Analytical methodology for TEX86 paleothermometry by high-performance liquid chromatography/atmospheric pressure chemical ionization-mass spectrometry, Anal Chem, 79, 2940-2944, 10.1021/ac062339v, 2007.
Schouten, S., Pitcher, A., Hopmans, E. C., Villanueva, L., van Bleijswijk, J., and Damste, J. S. S.: Intact polar and core glycerol dibiphytanyl glycerol tetraether lipids in the Arabian Sea oxygen minimum zone: I. Selective preservation and degradation in the water column and consequences for the TEX86, Geochimica Et Cosmochimica Acta, 98, 228-243, 10.1016/j.gca.2012.05.002, 2012.
Schouten, S., Hopmans, E. C., Rosell-Melé, A., Pearson, A., Adam, P., Bauersachs, T., Bard, E., Bernasconi, S. M., Bianchi, T. S., Brocks, J. J., Carlson, L. T., Castañeda, I. S., Derenne, S., Selver, A. D., Dutta, K., Eglinton, T., Fosse, C., Galy, V., Grice, K., Hinrichs, K.-U., Huang, Y., Huguet, A., Huguet, C., Hurley, S., Ingalls, A., Jia, G., Keely, B., Knappy, C., Kondo, M., Krishnan, S., Lincoln, S., Lipp, J., Mangelsdorf, K., Martínez-García, A., Ménot, G., Mets, A., Mollenhauer, G., Ohkouchi, N., Ossebaar, J., Pagani, M., Pancost, R. D., Pearson, E. J., Peterse, F., Reichart, G.-J., Schaeffer, P., Schmitt, G., Schwark, L., Shah, S. R., Smith, R. W., Smittenberg, R. H., Summons, R. E., Takano, Y., Talbot, H. M., Taylor, K. W. R., Tarozo, R., Uchida, M., van Dongen, B. E., Van Mooy, B. A. S., Wang, J., Warren, C., Weijers, J. W. H., Werne, J. P., Woltering, M., Xie, S., Yamamoto, M., Yang, H., Zhang, C. L., Zhang, Y., Zhao, M., and Damsté, J. S. S.: An interlaboratory study of TEX86and BIT analysis of sediments, extracts, and standard mixtures, Geochemistry, Geophysics, Geosystems, 14, 5263-5285, 10.1002/2013gc004904, 2013b.
Sikes, E. L., Volkman, J. K., Robertson, L. G., and Pichon, J. J.: Alkenones and alkenes in surface waters and sediments of the Southern Ocean: Implications for paleotemperature estimation in polar regions, Geochimica Et Cosmochimica Acta, 61, 1495-1505, 10.1016/S0016-7037(97)00017-3, 1997.
Smith, H. E. K., Poulton, A. J., Garley, R., Hopkins, J., Lubelczyk, L. C., Drapeau, D. T., Rauschenberg, S., Twining, B., Bates, N. R., and Balch, W. M.: The influence of environmental variability on the biogeography of coccolithophores and diatoms in the Great Calcite Belt, Biogeosciences, 14, 4905-4925, 10.5194/bg-14-4905-2017, 2017.
Strub, P. T., Mesías, J. M., Montecino, V., Rutllant, J., and Salinas, S.: Chapter 10. Coastal ocean circulation off western south america coastal segment, in: The Sea, edited by: Robinson, A. R., and Kenneth, H. B., 273-313, 1998.
Taylor, K. W. R., Huber, M., Hollis, C. J., Hernandez-Sanchez, M. T., and Pancost, R. D.: Re-evaluating modern and Palaeogene GDGT distributions: Implications for SST reconstructions, Global and Planetary Change, 108, 158-174, 10.1016/j.gloplacha.2013.06.011, 2013.
Toyos, M. H., Winckler, G., Arz, H. W., Lembke-Jene, L., Lange, C. B., Kuhn, G., and Lamy, F.: Variations in export production, lithogenic sediment transport and iron fertilization in the Pacific sector of the Drake Passage over the past 400 kyr, Climate of the Past, 18, 147-166, 10.5194/cp-18-147-2022, 2022.
Tyrrell, T. and Merico, A.: Emiliania huxleyi: bloom observations and the conditions that induce them, in: Coccolithophores, 75-97, 10.1007/978-3-662-06278-4_4, 2004.
Villanueva, L., Schouten, S., and Sinninghe Damste, J. S.: Depth-related distribution of a key gene of the tetraether lipid biosynthetic pathway in marine Thaumarchaeota, Environ Microbiol, 17, 3527-3539, 10.1111/1462-2920.12508, 2015.
Volkman, J. K.: Ecological and environmental factors affecting alkenone distributions in seawater and sediments, Geochemistry Geophysics Geosystems, 1, n/a-n/a, 10.1029/2000gc000061, 2000.
Vollmar, N. M., Baumann, K. H., Saavedra-Pellitero, M., and Hernandez-Almeida, I.: Distribution of coccoliths in surface sediments across the Drake Passage and calcification of Emiliania huxleyi morphotypes, Biogeosciences, 19, 585-612, 10.5194/bg-19-585-2022, 2022.
Vorrath, M. E., Muller, J., Rebolledo, L., Cardenas, P., Shi, X. X., Esper, O., Opel, T., Geibert, W., Munoz, P., Haas, C., Kuhn, G., Lange, C. B., Lohmann, G., and Mollenhauer, G.: Sea ice dynamics in the Bransfield Strait, Antarctic Peninsula, during past 240 years: a multi-proxy intercomparison study, Climate of the Past, 16, 2459-2483, 10.5194/cp-16-2459-2020, 2020.
Watson, A. J., Vallis, G. K., and Nikurashin, M.: Southern Ocean buoyancy forcing of ocean ventilation and glacial atmospheric CO2, Nature Geoscience, 8, 10.1038/Ngeo2538, 2015.

Weijers, J. W. H., Schouten, S., Spaargaren, O. C., and Damste, J. S. S.: Occurrence and distribution of tetraether membrane lipids in soils: Implications for the use of the TEX86 proxy and the BIT index, Organic Geochemistry, 37, 1680-1693, 10.1016/j.orggeochem.2006.07.018, 2006.

Wuchter, C., Schouten, S., Wakeham, S. G., and Sinninghe Damsté, J. S.: Temporal and spatial variation in tetraether membrane lipids of marine Crenarchaeota in particulate organic matter: Implications for TEX86paleothermometry, Paleoceanography, 20, 10.1029/2004pa001110, 2005.

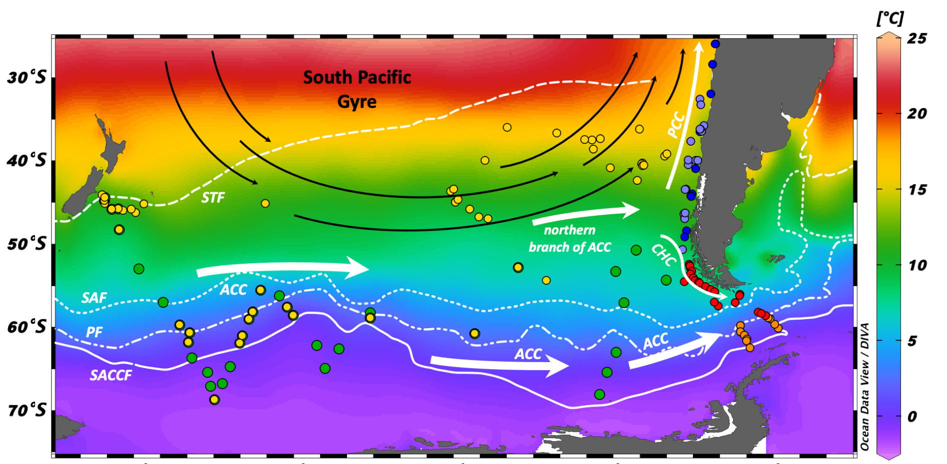

Figure 1: Map with SSTs (WOA05; Locarnini et al., 2006) of the extended study area and sample locations. ACC: Antarctic Circumpolar Current; PCC: Peru-Chile Current; CHC: Cape Horn Current; STF: Subtropical Front; SAF: Subantarctic Front; PF: Polar Front; SACCF: Southern ACC Front. Red dots: Southern Chilean Margin and Drake Passage samples (this study); Orange dots: Drake Passage samples (Lamping et al., 2021; this study); Light blue dots: Northern – Central Chilean Margin samples (Prahl et al., 2006; Prahl et al., 2010); Dark blue dots: Northern – Central Chilean Margin samples (Kaiser et al., 2015); Yellow dots: South Pacific Gyre, Central South Pacific and New Zealand Margin samples (Jaeschke et al., 2017); Green dots: Central South Pacific and New Zealand Margin samples (Ho et al., 2014).

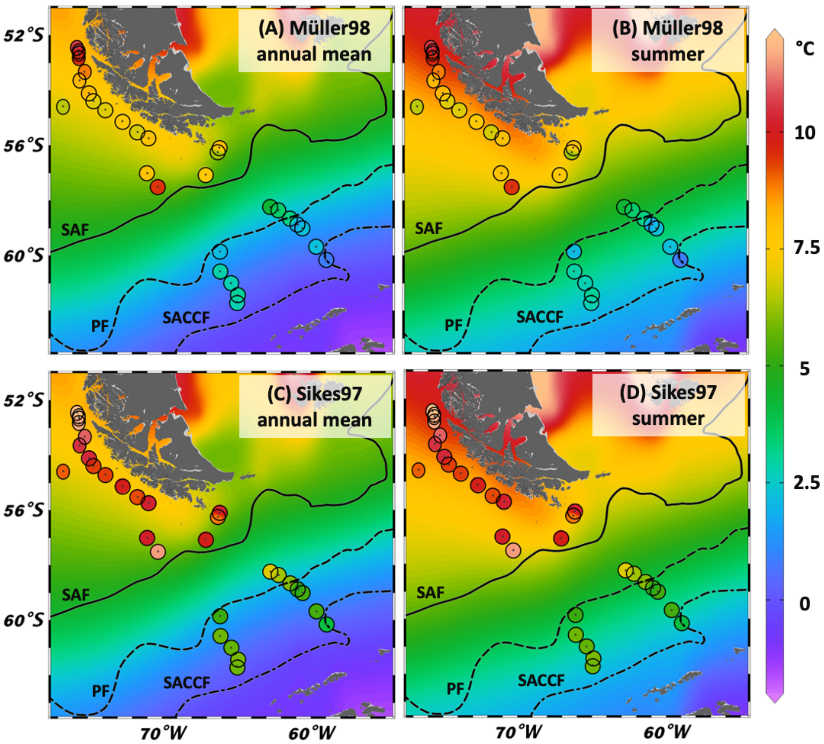

Figure 2: Map of reconstructed SST values for $U^{K'}_{37}$ (this study). Background gridded temperatures: WOA05 data (WOA05; Locarnini et al., 2006), colored dots are calculated SSTs. (A) WOA05 annual mean SSTs with Müller98 calibration; (B) WOA05 summer SSTs with Müller98 calibration; (C) WOA05 annual mean SSTs with Sikes97 calibration; (D) WOA05 summer SSTs with Sikes97 calibration.

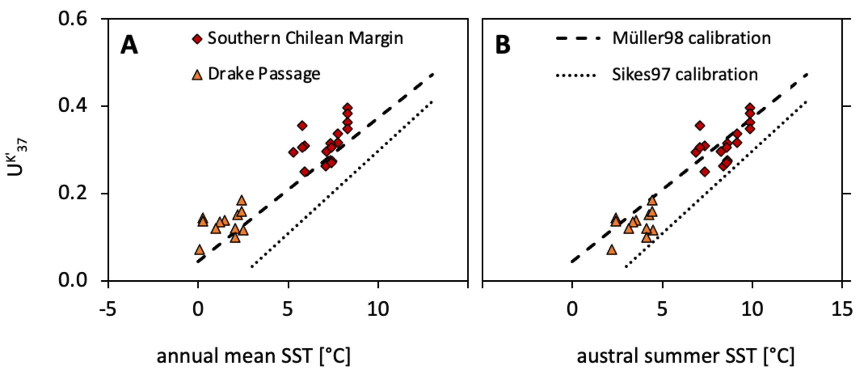

Figure 3: Comparison of $U^{K'}_{37}$ index (this study) with modern SSTs at 10 m water depth (WOA05; Locarnini et al., 2006), for (A) annual mean SSTs, and (B) austral summer SSTs, corresponding to January – March.

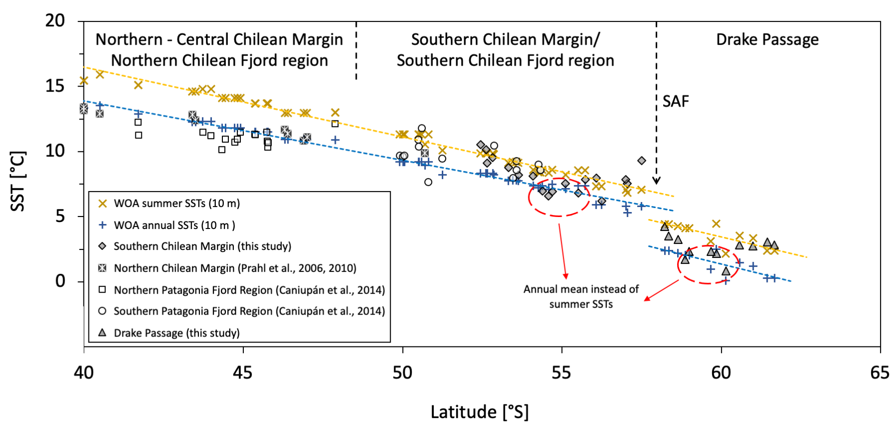

Figure 4: Comparison of ocean and fjord samples in the Chilean region. Yellow and Blue dashed lines show the meridional temperature evolution during summer and annual mean at 10 m water depth, respectively. Annual mean and summer data were taken from WOA09 (Locarnini et al., 2010) for the samples of Caniupán et al. (2014) and WOA05 (Locarnini et al., 2006) for Prahl et al. (2006, 2010) and this study.

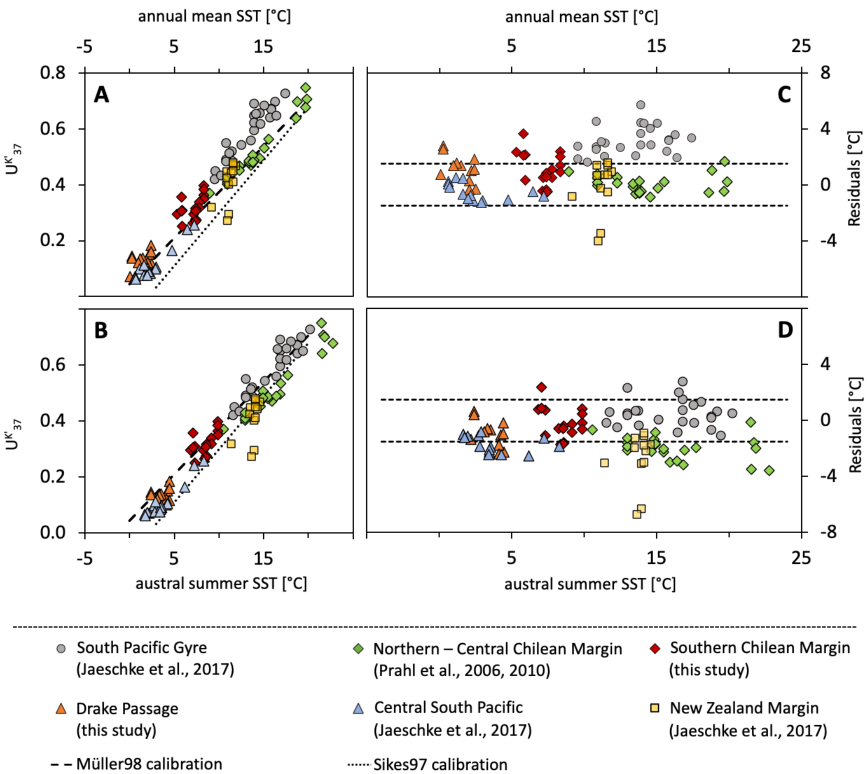

Figure 5: (A) and (B): Compilation of $U^{K'}_{37}$ index of this study and the expanded South Pacific study area with SSTs at 10 m water depth for annual mean and austral summer, respectively (WOA05; Locarnini et al., 2006). (C) and (D): Residuals of the local SSTs at 10 m water depth for the annual mean and austral summer (WOA05; Locarnini et al., 2006) subtracted by the Müller98 calculated SSTs. Temperature range of dotted line shows the standard error of the temperature calibration of ±1.5° C by Müller et al. (1998). Site PS75/088-6 (Jaeschke et al., 2017) was excluded due to unrealistic high temperatures of >10° C.

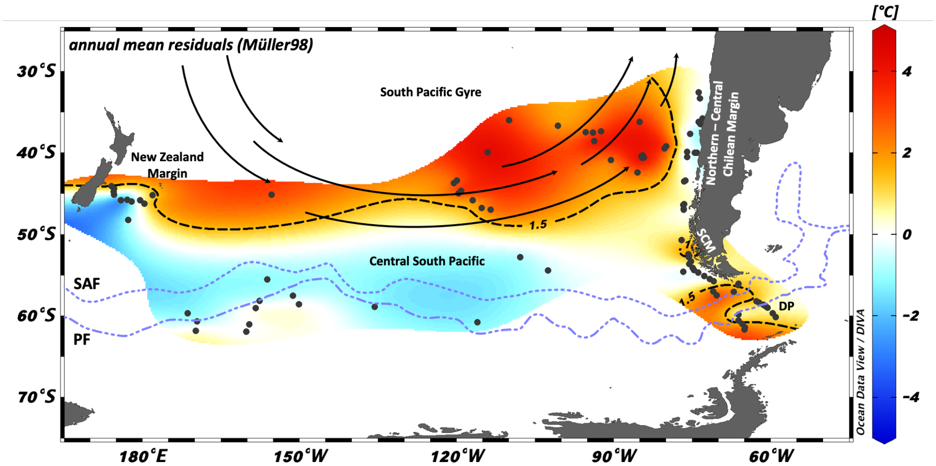

Figure 6: Map with residuals for the extended study area of the South Pacific with published data from the Central South Pacific, the New Zealand Margin, the South Pacific Gyre (Jaeschke et al., 2017) and the Chilean Margin (Prahl et al., 2006; this study; Prahl et al., 2010). Atlas-derived annual mean WOA05 water temperatures of 10 m water depth (Locarnini et al., 2006) were subtracted from the SST Müller98 calibration. SCM: Southern Chilean Margin; DP: Drake Passage; SAF: Subantarctic Front; PF: Polar Front.

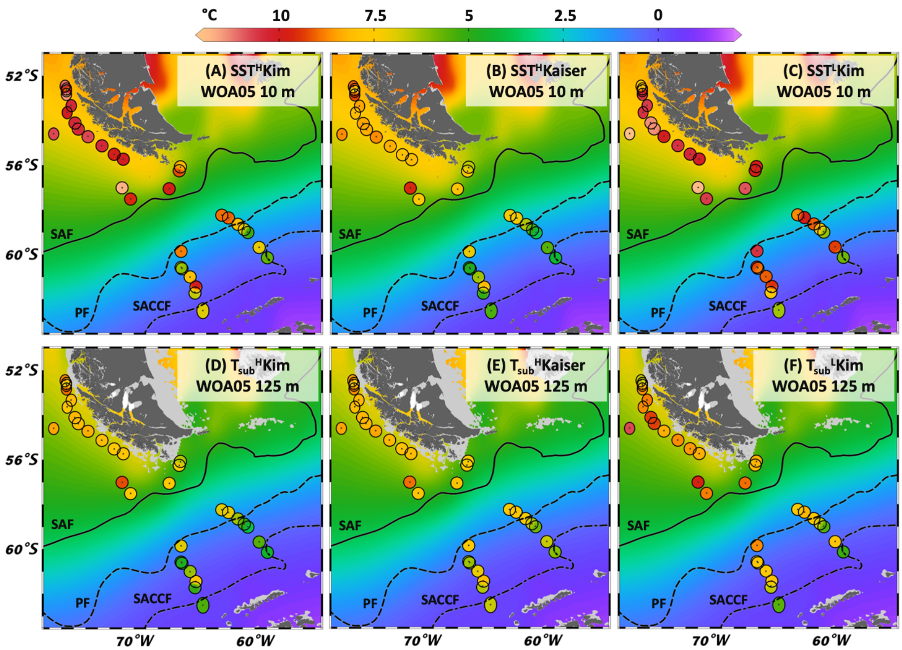

Figure 7: Map of reconstructed SST and Tsub values for TEX$^{H}_{86}$ and TEX$^{L}_{86}$ (this study). Background gridded annual mean temperatures at 10 or 125 m water depth: WOA05 data, colored dots are calculated SSTs or Tsub. (A) WOA05 SSTs with calculated data after SST^{H}Kim; (B) WOA05 SSTs with calculated data after SST^{H}Kaiser; (C) WOA05 SSTs with calculated data after SST^{L}Kim; (D) WOA05 Tsub with calculated data after Tsub^{H}Kim; (E) WOA05 Tsub with calculated data after Tsub^{H}Kaiser; (F) WOA05 Tsub with calculated data after Tsub^{L}Kim.

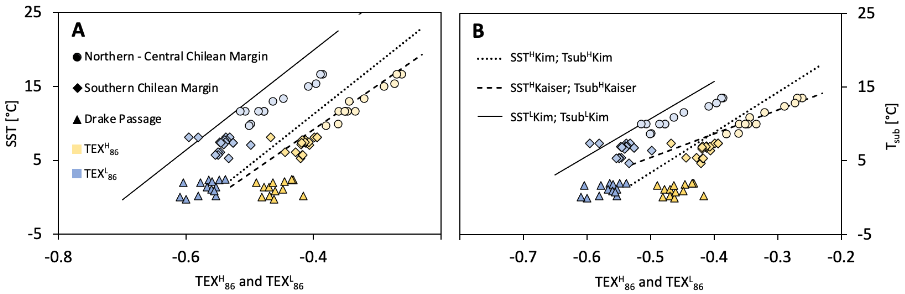

Figure 8: Comparison of TEX$^L_{86}$ (blue) and TEX$^H_{86}$ (yellow) data with water temperature with the SST 0 – 50 m water depth and Tsub 0 – 200 m (WOA05; Locarnini et al., 2006), respectively. Black line: TEX$^L_{86}$ calibration line (SST^{L}Kim, Tsub^{L}Kim) for surface and subsurface, respectively. Circles: Kaiser et al. (2015); Route: this study; triangle: Lamping et al. (2021) and this study.

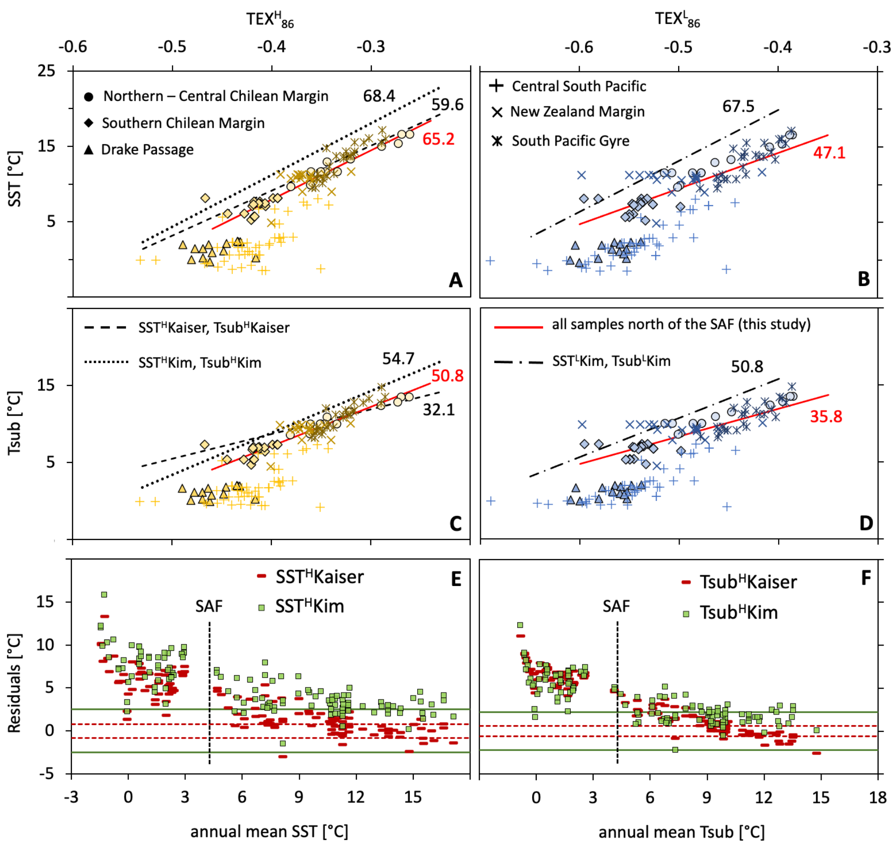

Figure 9: (A) – (D): Comparison of TEX^{H}_{86} (yellow) and TEX^{L}_{86} (blue) data with annual mean water temperature with the SST 0 – 50 m water depth and Tsub 0 – 200 m (WOA05; Locarnini et al., 2006), respectively. The black (previous studies) and red numbers (this study) indicate the slope of the corresponding calibration. Central South Pacific, New Zealand Margin and South Pacific Gyre samples: Ho et al. (2014) and Jaeschke et al. (2017); Northern – Central Chilean Margin samples: Kaiser et al. (2015); Southern Chilean Margin and Drake Passage samples: Lamping et al. (2021) and this study. (E) – (F): Residuals for SST 0 – 50 m and Tsub 0 – 200 m, with modern world ocean atlas-based temperatures (WOA05; Locarnini et al., 2006) subtracted from the calibrated temperatures. Green solid lines: standard error of ±2.5° C (SST^{H}Kim) and ±2.2° C ($Tsub^{H}$Kim). Red dashed lines: Calibration standard errors of ±0.8° C (SST^{H}Kaiser) and ±0.6° C ($Tsub^{H}$Kaiser).

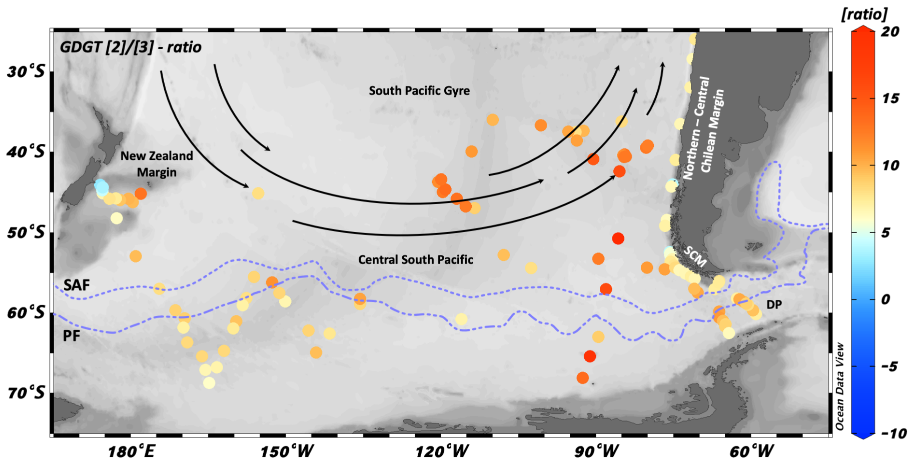

Figure 10: Map of GDGT [2]/[3]-ratios from our extended surface sediment sample set across different regions within the study area. SCM: Southern Chilean Margin; DP: Drake Passage; SAF: Subantarctic Front; PF: Polar Front.

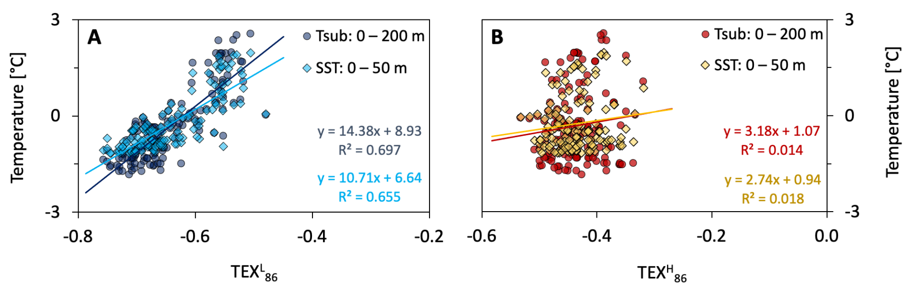

Figure 11: TEX^H_{86} and TEX^L_{86} Indices south of the SAF vs. modern WOA05 water temperatures. (A) TEX^L_{86} of all South Pacific samples; (B) TEX^H_{86} of all South Pacific samples.

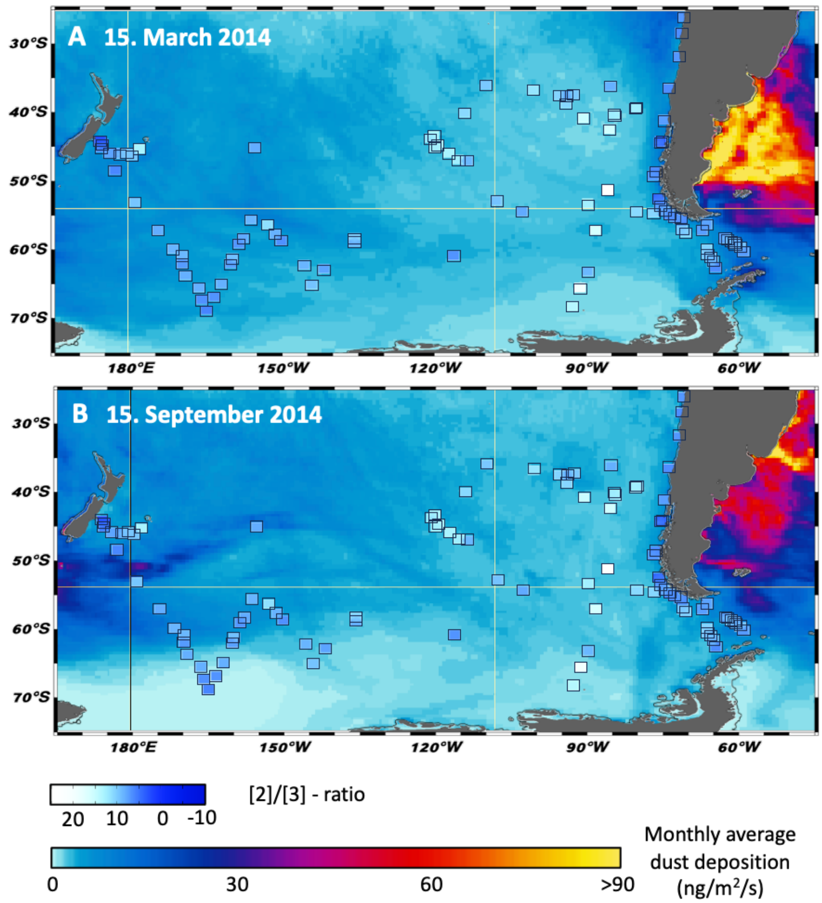

799

800 **Figure 12: GDGT [2]/[3]-ratio on a map, showing total monthly average dust deposition (dry + wet) for the times (A) march 2014**
801 **and (B) September 2014. Dust data were taken from NASA worldview (Global_Modeling_and_Assimilation_Office_(Gamo), 2015).**

802

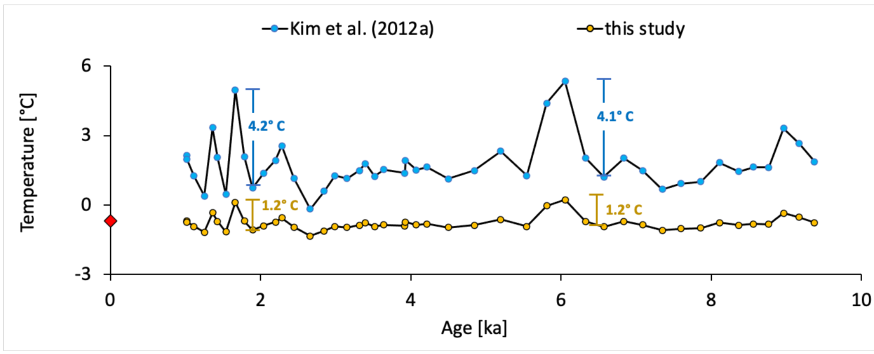

Figure 13: Comparison of core MD03-2601 (Kim et al., 2012b) with the temperature calibration Tsub^{L}Kim (blue) and the new subsurface calibration of this study (yellow). Red dot marked the mean temperature of 0 – 200 m water depth at the coring site.

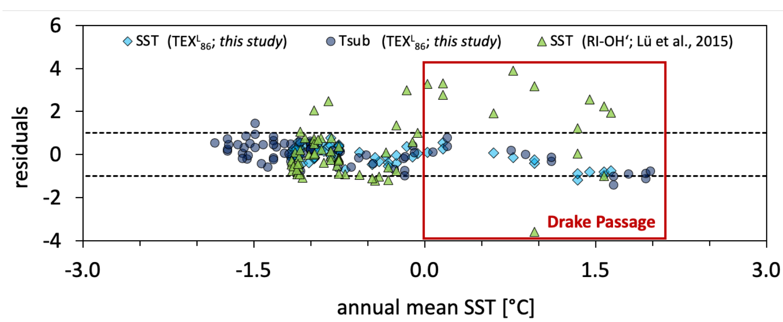

Figure 14: Residuals for SST 0 – 50 m and Tsub 0 – 200 m, with modern world ocean atlas-based temperatures (WOA05; Locarnini et al., 2006) subtracted from the calibrated temperatures. Black dashed lines mark the 1° C and -1° C isotherm, respectively.